# The entwined wiggling of homoclinic curves emerging from saddle-node/Hopf instabilities

A.R. Champneys [a] V. Kirk [b]

[a] *Department of Engineering Mathematics, University of Bristol, Bristol BS8 1TR, UK*

[b] *Department of Mathematics, University of Auckland, Private Bag 92019, Auckland, New Zealand*

**Abstract**

An analysis is presented of the homoclinic bifurcations occurring in a generic unfolding of a saddle-node/Hopf singularity (also known as a Gavrilov-Guckenheimer point). Specifically, an explanation is given of previously numerically observed oscillations of loci of homoclinic orbits to two different saddle focus equilibria. These oscillation occur within an exponentially thin wedge of parameter space that emerges from the codimension-two point. The frequency of oscillation tends to zero as the codimension-two point is approached. Earlier theory by Gaspard showed that homoclinic orbits must exist inside the parameter wedge. This result is here extended to give the frequency and amplitude of the oscillations of the homoclinic loci within the wedge. It is also shown how the two loci are related to each other, and, in the case of only cubic perturbations of the normal form, that they are precisely out of phase. The analysis is shown to agree with numerical results on perturbed normal forms and in two model systems arising in applications to atmospheric dynamics and to calcium wave propagation.

*Key words:* codimension-two point, saddle-node/Hopf, Shil'nikov homoclinic orbit, beyond all orders
*PACS:* 02.30.Hq 02.30.Oz

## 1 Introduction

A frequently used tool in the analysis of the dynamics associated with a parametrised system of differential equations is the construction of a bifurcation set showing the location of bifurcations of the system as one or more parameter is varied. When the system has two or more parameters it is common to draw two-parameter bifurcation sets; in this context, codimension-

one bifurcations are located on one-dimensional curves in the bifurcation set and codimension-two bifurcations occur at isolated points. The codimension-two points can be regarded as organising centres for the bifurcation set, with several curves of codimension-one bifurcations typically emerging from each codimension-two point. Thus, an understanding of common codimension-two bifurcations is of great help in the study of systems with two or more parameters.

One of the simplest codimension-two bifurcations is the saddle-node/Hopf (SNH) instability, where there is simultaneously a saddle-node bifurcation and a Hopf bifurcation, so that the linearisation of the vector field evaluated at an equilibrium solution and restricted to the centre manifold has eigenvalues $0, \pm i\omega$. The dynamics associated with the SNH instability has been extensively studied; overviews of results are given in [10,13], with further results and references in [7,12]. The normal form for the bifurcation can be written as:

$$\dot{q} = q\,(\lambda + i\omega + \sum_{2m+n\geq 1} \alpha_{m,n}|q|^{2m} z^n), \tag{1.1}$$

$$\dot{z} = \mu + \sum_{2m+n\geq 2} \gamma_{m,n}|q|^{2m} z^n, \tag{1.2}$$

where $q, \alpha_{m,n} \in \mathbb{C}$, $z, \gamma_{m,n} \in \mathbb{R}$ and $\lambda, \mu \in \mathbb{R}$ are unfolding parameters. Depending on the signs of the coefficients $\alpha_{0,1}$ and $\gamma_{0,2}$ (assuming, without loss of generality, that $\gamma_{1,0} = -1$), four qualitatively different cases of the normal form can be identified [10,13]. In two of these cases, the dynamics seen in unfoldings of the normal form is straightforward, consisting just of fixed points and periodic orbits arising through the primary saddle-node and Hopf bifurcations. In the other two cases, there are additional secondary bifurcation resulting from the interaction of the primary bifurcations, and the dynamics near the co-dimension two bifurcation can be quite complicated. This paper shall explicitly involve one of the latter cases; $\alpha_{0,1} > 0$, $\gamma_{0,2} < 0$.

The normal form (1.1), (1.2) is equivariant with respect to an $S^1$ symmetry, corresponding to cylindrical symmetry about the $z$-axis, which renders the dynamics to be effectively planar. This symmetry is a result of the procedure of reduction to normal form; there is a nonlinear change of coordinates that will remove nonresonant terms up to any given finite order, leaving just symmetric terms in the normal form. However, when faced with a true example system undergoing a saddle-node/Hopf bifurcation, it will not in general possess this symmetry. The normal form procedure can impose this symmetry up to any finite order, by removal of all non-resonant terms, but symmetry-breaking terms will always be present beyond all algebraic orders. In other words, the normal form (1.1), (1.2) is not a *topological normal form* [13] (or *versal unfolding* [10]) of the bifurcation.

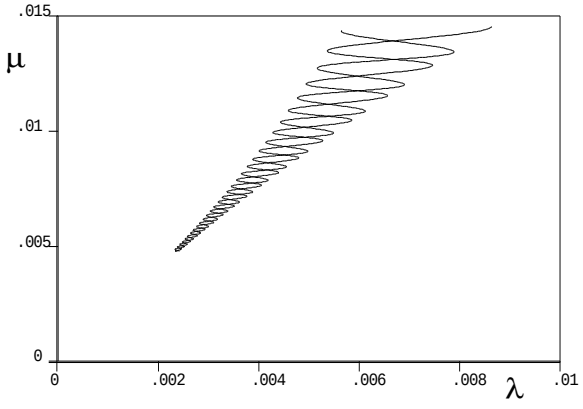


Fig. 1. Entwined wiggling of homoclinic bifurcations of saddle-foci in a cubic perturbation of the saddle-node/Hopf normal form, after [12], see Sec. 4.1 below.

Thus, to fully understand the dynamics associated with this instability, it is necessary to consider the effect of breaking the normal form symmetry. It is also most desirable to keep the symmetry-breaking terms at the lowest order possible. Specifically, they should enter at the next order to the truncated normal form of lowest order necessary to describe the steady state bifurcations in the system. In this case, we consider symmetry-breaking perturbations that are to lowest order cubic; see (2.1), (2.2) below.

Several authors have shown that, in the absence of the normal form symmetry, there may be homoclinic and heteroclinic bifurcations and chaotic dynamics occurring arbitrarily close to a SNH bifurcation point (see, for example, [4,7,9]). In particular Gaspard [7] showed that, in the case under consideration here, homoclinic bifurcations of Shil'nikov type must occur near the codimension-two point, lying inside a thin wedge of parameter space emanating from the codimension-two point. He further showed that, in the case of purely cubic perturbations to the normal form, the wedge is in fact exponentially thin, and he computed a linear approximation to it. Other dynamical features can be seen to occur inside this wedge including chaotic attractors, heteroclinic tangencies, and the merging of resonance tongues; see e.g. [4,12].

In a numerical study of the perturbed normal form, Kirk [12] noticed that within the wedge, there are loci of primary homoclinic bifurcations involving two different equilibria, with these loci displaying a distinctive entwined oscillation about each other – see Fig. 1. Similar wiggly homoclinic bifurcation curves have also been observed in systems arising from applications in which SNH bifurcations occur as part of a larger bifurcation set. For example, Balmforth et al. [1] found just such an oscillatory curve of Shil'nikov homoclinic bifurcations, and (erroneously) conjectured that the additional structure gained by the homoclinic loop as it traverses a wiggle in parameter space is caused by an additional local bifurcation. Also, Shil'nikov, Nicolis & Nicolis

[16] studied a certain third-order atmospheric model due to Lorenz (a modification of his famous equations), and found two highly-oscillatory branches of homoclinic bifurcations emerging from the codimension-two point. Interestingly, one of these branches has the property that as it oscillates it repeatedly collides with a branch of saddle-node bifurcations causing codimension-two non-central saddle-node bifurcations. More recently, van Veen *et al.* [21] have found the same homoclinic branches occurring in a more accurate, higher-order model of the same atmospheric phenomenon. Similar wiggly curves have been found in different models of chaotic lasers, e.g. [18]. Finally we mention a problem in the study of intracellular calcium wave propagation, where pulses in calcium concentration correspond to Shil'nikov-type homoclinic orbits of a system of travelling-wave ordinary differential equations [20]. In a plot of wave speed versus system parameter, a branch of travelling waves is found to approach a SNH point via oscillation within a thin wedge, in the same way as in the examples above. Recently a second branch of homoclinic orbits to another equilibrium has also been found in this model, forming the entwined partner to the first branch of homoclinic orbits [19]. A feature of particular interest in this model is that at the other end of the main homoclinic branch (i.e., not at its limit at the SNH point), the homoclinic orbits arise as the gluing together of two *unstable* fronts, and yet can be shown to give rise to *stable* pulses of the underlying partial differential equation [15].

The ubiquitous and regular nature of the numerically observed wiggly homoclinic bifurcations suggests that some underlying generic feature of the instability is causing the wiggling, but until now, there seems to have been no explanation of this feature of the dynamics. The purpose of this paper then, is to present a rational explanation of this characteristic wiggling emanating from the SNH instability of the type ($\alpha_{0,1} > 0, \gamma_{0,2} < 0$), which has been seen repeatedly in examples. In particular, we shall obtain precise estimates of the frequency and amplitude of the oscillations ('wiggles') of the two primary homoclinic bifurcation curves emerging from the codimension-two point and show how the bifurcation curves are related to each other.

In section 2, we describe the dynamics associated with the normal form for the case of the SNH bifurcation that we are interested in. In section 3, we first summarise some results of Gaspard [7]. Then we show how his perturbation analysis can be extended to yield estimates for the amplitude and frequency of the oscillations, first in the case of cubic perturbations to the normal form, and then for arbitrary analytic perturbations. In section 4 we compare the predictions of our analysis with numerical results from the perturbed normal form equations and from two model systems arising in applications to atmospheric dynamics and to calcium wave propagation. Conclusions are given in section 5. Our analytic results depend on knowing the asymptotic behaviour of certain integrals, the calculation of which is given in Appendix A. Appendix B contains some technical details of the convergence of a particular power series

we use in our calculations.

## 2 Saddle-node/Hopf normal form and its perturbation.

After appropriate co-ordinate transformations, any sufficiently smooth three-dimensional system in a neighbourhood of a SNH bifurcation point may be written in the form of the truncated unfolded normal form plus higher-order terms:

$$\dot{q} = (\lambda + i\omega)q + (\alpha + i\beta)zq + F(q, \overline{q}, z), \tag{2.1}$$
$$\dot{z} = \mu - z^2 + s|q|^2 + G(q, \overline{q}, z), \tag{2.2}$$

for $z \in \mathbb{R}$, $q \in \mathbb{C}$. Here $\lambda$ and $\mu$ unfold the Hopf and saddle-node bifurcations respectively, $s = \pm 1$, and $\alpha \neq 0$, $\beta$ and $\omega > 0$ are normal-form parameters that may be further simplified if necessary by rescaling of time and co-ordinates. The functions $F \in \mathbb{C}$ and $G \in \mathbb{R}$ are assumed to be analytic, that is, their Taylor series

$$F(q, \overline{q}, z) = \sum_{j+k+l \geq 3} c_{jkl} q^j \overline{q}^k z^l, \qquad G(q, \overline{q}, z) = \sum_{j+k+l \geq 3} d_{jkl} q^j \overline{q}^k z^l \tag{2.3}$$

converge for all $(q, z)$ in some sufficiently large ball $B(0, 0)$. In general, $c_{jkl}, d_{jkl} \in \mathbb{C}$, but owing to the requirement that $G$ be real we have

$$d_{jkl} = \overline{d}_{kjl}, \qquad d_{00l} \in \mathbb{R}. \tag{2.4}$$

Note that the terms in $F$ proportional to $c_{jkl}$ with $j = k + 1$ and those in $G$ proportional to $d_{jkl}$ with $k = j$ are resonant terms which are present in the normal form (1.1),(1.2).

The second-order truncated normal form (henceforth referred to as the *truncated system*) is obtained by setting $F = G \equiv 0$ in (2.1), (2.2). Its dynamics is well understood [10,13]. Four cases can be identified, from the combinations of the signs of $s$ and $\alpha$. We consider the case that $\alpha > 0$ and $s = -1$, in which case upon setting $q = re^{i\phi}$, the truncated system reduces to

$$\begin{aligned} \dot{r} &= \lambda r + \alpha r z \,, \\ \dot{z} &= \mu - z^2 - r^2 \,, \\ \dot{\phi} &= \omega + \beta z \,. \end{aligned} \tag{2.5}$$

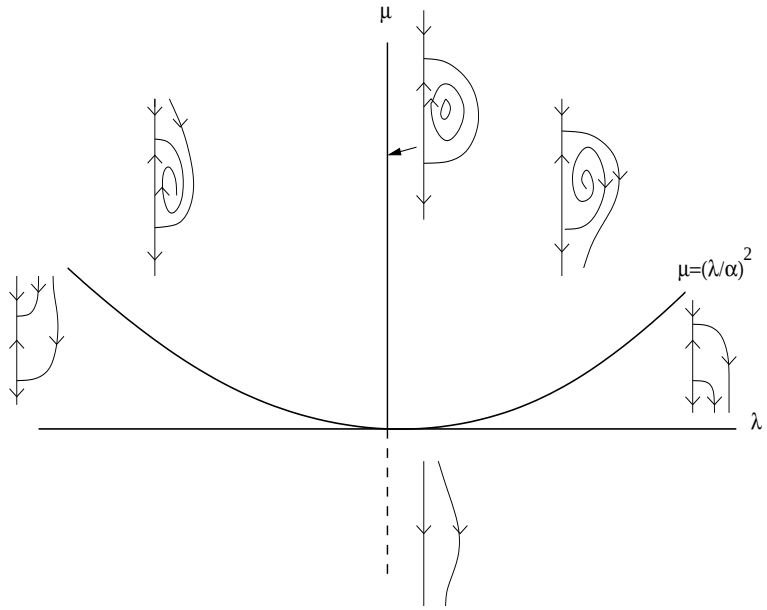


Fig. 2. Bifurcation set and phase portraits for the truncated normal form (2.5), after [10]. Phase portraits have $r$ on the horizontal axis, $z$ on the vertical axis; to recover three-dimensional phase portraits, rotate each phase portrait about the $z$-axis.

Note that the equations for $\dot{r}$ and $\dot{z}$ are independent of $\phi$, which implies that the truncated system is equivariant with respect to rotations about the $z$-axis. Without loss of generality, we may assume that $\beta = 0$. This follows from making a near-identity rescaling of time (for $z \ll \beta/\omega$)

$$t_{\rm new} = t_{\rm old}(1 + \beta z/\omega), \tag{2.6}$$

then a redefinition of $z$

$$z_{\rm new} = z_{\rm old} + \frac{\mu\beta}{2\omega}\,. \tag{2.7}$$

Substituting these formulae into (2.5) we recover (up to quadratic order in $(\mu, \lambda, z, r)$) equations of the form of (2.5) but with

$$\beta_{\rm new} = 0, \qquad \alpha_{\rm new} = \alpha_{\rm old} - \lambda_{\rm old}\beta_{\rm old}/\omega, \tag{2.8}$$

and $\lambda$ and $\mu$ re-defined as

$$\lambda_{\rm new} = \lambda_{\rm old} - \frac{\alpha_{\rm old}\mu_{\rm old}\beta_{\rm old}}{2\omega} + \text{h.o.t.}, \qquad \mu_{\rm new} = \mu_{\rm old} - \frac{\mu_{\rm old}^2\beta_{\rm old}^2}{4\omega^2} + \text{h.o.t.}$$

Note that this transformation leads to a rescaled definition of the coefficients $c_{ijk}$, $d_{ijk}$, obtained by applying the transformation (2.6), (2.7) to the Taylor

series expansions for $F$ and $G$. Henceforth then, we assume $\beta = 0$ without loss of generality.

The dynamics of the truncated system is summarised in Fig. 2. There exist two fixed points for positive $\mu$ which are born in a saddle-node bifurcation at $\mu = 0$. These are given by

$$P_\pm : \qquad (q, z) = (0, \pm\sqrt{\mu}),$$

which have eigenvalues

$$\lambda + \alpha\sqrt{\mu} \pm i\omega, \quad -2\sqrt{\mu}, \qquad \text{for } P_+,$$

$$-\lambda - \alpha\sqrt{\mu} \pm i\omega, \quad 2\sqrt{\mu}, \qquad \text{for } P_-.$$

Thus, when $|\lambda| < \alpha\sqrt{\mu}$, $P_+$ has a two-dimensional unstable manifold and a one-dimensional stable manifold, while $P_-$ has a two-dimensional stable manifold and a one-dimensional unstable manifold.

When $\lambda = 0$, the system is conservative with a constant of the motion

$$H = \frac{1}{2}\alpha|q|^{2/\alpha}\left(\frac{|q|^2}{\alpha+1} + z^2 - \mu\right).$$

In this case the two equilibria are connected in a heteroclinic cycle, which corresponds to the choice $H = 0$. This cycle is comprised of [7]: a one-dimensional connection from $P_-$ to $P_+$ formed from one component of the stable manifold of $P_+$

$$W_s(P_+): \quad q_{s0}(t) = 0, \tag{2.9}$$
$$z_{s0}(t) = \sqrt{\mu}\tanh\sqrt{\mu}t\,; \tag{2.10}$$

and a two-dimensional surface of connections which is the entire unstable manifold of $P_+$

$$W_u(P_+): \quad q_{u0}(t) = \sqrt{\mu}(\alpha+1)^{1/2}\frac{e^{i(\theta+\omega t)}}{\cosh(-\alpha\sqrt{\mu}t)}, \tag{2.11}$$
$$z_{u0}(t) = \sqrt{\mu}\tanh\left(-\alpha\sqrt{\mu}t\right). \tag{2.12}$$

Here the parameter $\theta \in [0, 2\pi)$ parametrises individual trajectories in the two-dimensional manifold, $W_u(P_+)$.

The work of Gaspard [7] involves unfolding this structurally unstable heteroclinic connection for the full system and showing that homoclinic connections from either $P_+$ or $P_-$ to itself are inevitable (see Fig. 3). He shows that, in the presence of only cubic terms in the perturbations $F$ and $G$, such connections

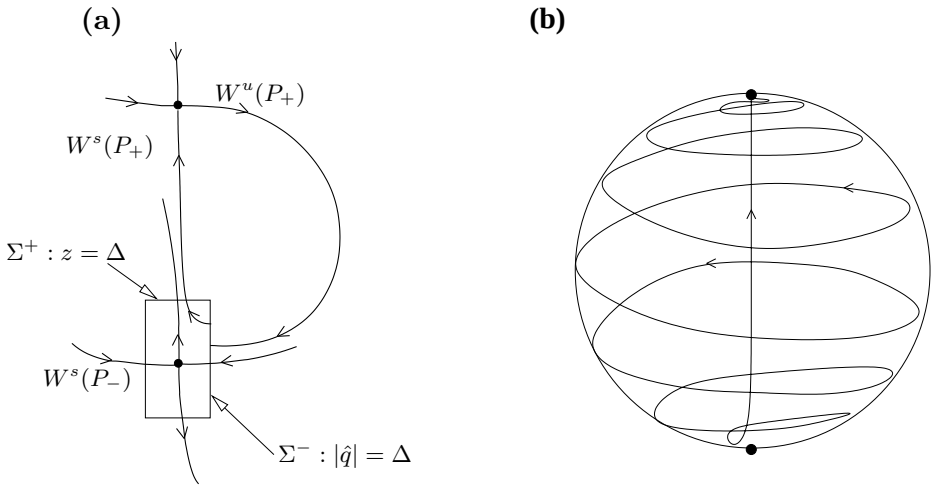


Fig. 3. The unfolding of the structurally unstable heteroclinic cycle; (a) schematic representation of the stable and unstable manifolds of $P_+$ and $P_-$, also showing the sets $\Sigma^{\pm}$ used later; (b) possible homoclinic orbit to $P^+$ in the unfolding.

occur within a certain exponentially thin wedge of the $(\lambda, \mu)$-plane. We shall adopt his approach to further reveal the precise asymptotic behaviour of these loci of homoclinic connections under arbitrary analytic perturbations $F$ and $G$.

## 3 Asymptotics of the homoclinic curves

In this section we adopt the perturbation method used in [7] to find explicit formulae for the loci of the primary homoclinic bifurcations of $P_+$ and $P_-$ in the limit of small $\mu$. To be concrete, consider first homoclinic connections to $P_+$. We then start (Sec. 3.1) by finding expressions for the stable and unstable manifolds of $P_+$ and then (Sec. 3.2) determine the intersections of these manifolds in the limit $\mu \to 0$ in the presence of purely cubic terms in $F$ and $G$. By keeping careful track of the phase dependence of the beyond-all-orders part of this intersection, we are then able in Sec. 3.3 to extend Gaspard's analysis in order to obtain asymptotic expressions for the amplitude and frequency of the oscillations of the homoclinic bifurcation curve. Section 3.4 considers the extra effects brought about by arbitrary, not necessarily cubic, perturbations $F$ and $G$. All terms in the Taylor series expansions of $F$ and $G$ are found to contribute to the required integrals at the *same* order, but our results are qualitatively unchanged by the inclusion of higher-order terms. Finally, Sec. 3.5 considers a simple transformation of the coordinates and coefficients in (2.1),(2.2) to obtain the locus of homoclinic connections to $P_-$ immediately from our expressions calculated for $P_+$.

We note that there are two necessary conditions for the existence of homoclinic

orbits of the fixed points $P_+$ and $P_-$: that the $z$-axis in the phase space not be dynamically invariant and that the two-dimensional manifolds $W^u(P_+)$ and $W^s(P_-)$ not be coincident. The former condition is satisfied only if $c_{00l} \neq 0$ in (2.3) for some $l \geq 3$, in which case the latter condition is also satisfied. We henceforth assume that at least one of the $c_{00l}$ is non-zero in the perturbations we take.

### *3.1 Perturbed stable and unstable manifolds*

The key idea is to consider as independent perturbations $\lambda \neq 0$ and a fictitious parameter $\epsilon > 0$ that multiplies both $F$ and $G$, and then to perform a generalised Melnikov analysis with respect to these two parameters; this process allows the calculation of first-order correction terms to the one- and two-dimensional heteroclinic connections $(q_{s0(t)}, z_{s0}(t))$ and $(q_{u0}(t), z_{s0}(t))$. In truth $\varepsilon$ should be set to unity, but note that it can be seen as a book-keeping parameter since $q, z = O(\sqrt{\mu})$ for the solutions of interest and therefore $F, G = O(\mu^{3/2})$ to leading order. See [7, Sec. 3] for more details.

It is straightforward to see that the perturbed equilibria can be written as

$$P_\pm : \quad q_\pm = \frac{-F(0,0,\pm\sqrt{\mu})}{i\omega \pm \alpha\sqrt{\mu}}, \quad z_\pm = \pm\sqrt{\mu} \pm \frac{G(0,0,\pm\sqrt{\mu})}{2\sqrt{\mu}},$$

for all $\lambda$. A careful calculation following the procedure described in [7] then gives the following leading-order asymptotic expressions for the first-order corrections to the stable and unstable manifolds of $P_+$ as they approach the equilibrium $P_-$.

For the one-dimensional manifold:

$$\text{as } t \to -\infty \qquad z_{s\lambda} \to 0 \tag{3.1}$$

$$q_{s\lambda} \to 0 \tag{3.2}$$

$$z_{s\varepsilon} \sim -\frac{G(0,0,-\sqrt{\mu})}{2\sqrt{\mu}} \tag{3.3}$$

$$q_{s\varepsilon} \sim q_- - \frac{I_s}{2^\alpha} e^{i\omega t - \alpha\sqrt{\mu}t}, \tag{3.4}$$

where

$$I_s = \int_{-\infty}^{\infty} d\tau F(0,0,z_{s0}) \frac{e^{-i\omega\tau}}{(\cosh\sqrt{\mu}\tau)^\alpha}, \tag{3.5}$$

and subscripts $s\lambda$ and $s\varepsilon$ refer to the first-order corrections to $(q_{s0}, z_{s0})$ with

respect to the two perturbation parameters.

For the two-dimensional manifold:

$$\text{as } t \to +\infty \qquad z_{u\lambda} \sim -\frac{I_\lambda e^{2\sqrt{\mu}t}}{(2\sqrt{\mu})^{1+2/\alpha}(1+\alpha)^{1+1/\alpha}} \tag{3.6}$$

$$q_{u\lambda} \sim -\frac{\alpha I_\lambda e^{i\theta} e^{i\omega t+(2-\alpha)\sqrt{\mu}t}}{\left(2\sqrt{\mu(1+\alpha)}\right)^{1+2/\alpha}}$$

$$z_{u\varepsilon} \sim -\frac{G(0,0,-\sqrt{\mu})}{2\sqrt{\mu}} - \frac{I_u(\theta)e^{2\sqrt{\mu}t}}{(2\sqrt{\mu})^{1+2/\alpha}(1+\alpha)^{1+1/\alpha}} \tag{3.7}$$

$$q_{u\varepsilon} \sim q_- - \frac{\alpha I_u(\theta) e^{i\theta} e^{i\omega t+(2-\alpha)\sqrt{\mu}t}}{\left(2\sqrt{\mu(1+\alpha)}\right)^{1+2/\alpha}},$$

where

$$I_\lambda = 2\int_{-\infty}^{\infty} d\tau |q_{u0}|^{2+2/\alpha}, \tag{3.8}$$

$$I_u(\theta) = 2\int_{-\infty}^{\infty} d\tau |q_{u0}|^{2/\alpha}(\mathrm{Re}(\overline{q}_{u0}F_{u0}) + (1+\alpha)z_{u0}G_{u0}), \tag{3.9}$$

and a subscript $u0$ on $F$ or $G$ refers to their evaluation at $(q,z) = (q_{u0}, z_{u0})$.

The key to what follows is the asymptotics of the integrals $I_u$, $I_s$ and $I_\lambda$ as $\mu \to 0$.

### *3.2 Asymptotic behaviour of $I_u$, $I_s$ and $I_\lambda$ as $\mu \to 0$*

The integral $I_\lambda$ is by definition independent of $F$ and $G$. The integrals $I_{s,u}$ do depend on the form of $F$ and $G$. Hence we may write

$$I_{s,u} = I_{s,u}^{(3)} + I_{s,u}^{(4)} + I_{s,u}^{(5)} + \dots$$

where the superscript $(n)$ refers to taking only $n$th-order ($j+k+l=n$) terms in the Taylor expansions (2.3) of $F$ and $G$. For simplicity as in [7,11], we initially consider only the effects of the cubic terms in $F$ and $G$; that is replace $I_{s,u}$ by $I_{s,u}^{(3)}$. Later, in Sec. 3.4, we show that higher-order terms in $F$ and $G$ essentially do not change the arguments that follow, provided adjustments are made to the definition of certain constants.

The following asymptotic relation as $\mu \to 0$ will be helpful (see Appendix A):

$$\int_{-\infty}^{\infty} d\tau \frac{[\sinh(\tau)]^p}{[\cosh(\tau)]^\Lambda} e^{i\frac{K\tau}{\sqrt{\mu}}} \sim 2\pi (i\,\mathrm{sgn}(K))^p \left(\frac{|K|}{\sqrt{\mu}}\right)^{\Lambda-1} \frac{1}{\Gamma(\Lambda)}\, e^{-\frac{|K|\pi}{2\sqrt{\mu}}}, \quad (3.10)$$

where $p$ is a non-negative integer, $\Lambda > p$ but is in general non-integer, and $K \neq 0$ is a real constant that is independent of $\mu$. Also, we have [6,8]

$$\int_{-\infty}^{\infty} \frac{d\tau}{[\cosh(\tau)]^\Lambda} = B(1/2, \Lambda/2) = \sqrt{\pi}\frac{\Gamma(\frac{\Lambda}{2})}{\Gamma(\frac{1+\Lambda}{2})}. \quad (3.11)$$

Consider first the integral $I_\lambda$. Upon substitution of (2.11) into (3.8), and making use of relation (3.11), one obtains (cf. [7, eq. (4.4)])

$$I_\lambda = 2\sqrt{\pi}\sqrt{\mu}^{1+2/\alpha}(\alpha+1)^{1/\alpha}\frac{\Gamma(2+1/\alpha)}{\Gamma(3/2+1/\alpha)}, \quad (3.12)$$

which is real and positive.

Next consider $I_s^{(3)}$. From the definition (3.5) note that $I_s^{(3)}$ consists of a single term

$$I_s^{(3)} = c_{003}\mu \int_{-\infty}^{\infty} d\tau \frac{[\sinh(\tau)]^3}{[\cosh(\tau)]^{3+\alpha}} e^{-i\frac{\omega\tau}{\sqrt{\mu}}}.$$

Hence, using relation (3.10), we find that as $\mu \to 0$

$$I_s^{(3)} \sim 2\pi i\, \frac{c_{003}\mu}{\Gamma(3+\alpha)} \left(\frac{\omega}{\sqrt{\mu}}\right)^{2+\alpha} e^{\frac{-\omega\pi}{2\sqrt{\mu}}}, \quad (3.13)$$

which is exponentially small in $\mu$.

Finally, consider $I_u^{(3)}$. This consists of several terms, one for each coefficient $c_{jkl}$ and $d_{jkl}$ with $j+k+l=3$. However, certain of these terms lead to integrals that are asymptotically smaller than others. In particular, note from the form of $q_{u0}$ and $z_{u0}$ in (2.11) and (2.12), that those terms in the integrand of (3.9) that are functions of $|q|$ and $z$ (and hence do not break the circular symmetry of the normal form), do not have any exponential factor in the integrand. These terms come from monomials in $F$ and $G$ with coefficients

$$c_{102}, \quad c_{210}, \quad d_{003}, \quad d_{111}, \quad (3.14)$$

which are the resonant terms present in the cubic truncated normal form.

Each of the corresponding terms in $I_u$ leads to an integral of the form (3.11), which may be seen by making the substitution

$$\tau = \alpha\sqrt{\mu}t, \tag{3.15}$$

and using the expansion of even powers of $\sinh\tau$ in terms of $\cosh\tau$. Let this non-exponentially small portion of the integral be termed $I_{u0}^{(3)}$. Repeated use of (3.11) and some manipulation of the $\Gamma$ functions yields

$$I_{u0}^{(3)} = \sqrt{\mu}^{3+2/\alpha} K_0^{(3)} \sqrt{\pi}(1+\alpha)^{1/\alpha} \frac{\Gamma(2+1/\alpha)}{\Gamma(3/2+1/\alpha)}, \tag{3.16}$$

where

$$K_0^{(3)} = \frac{1}{3\alpha+2}(2\alpha \mathrm{Re}\, c_{102} + 4(\alpha+1)^2 \mathrm{Re}\, c_{210} + 3\alpha^2 d_{003} + 2\alpha(\alpha+1)d_{111}). \tag{3.17}$$

Given the form of (2.11) and (2.12), note that all cubic terms in $F$ and $G$ other than (3.14) lead to terms in the integrand of $I_u^{(3)}$ that contain $e^{i(\theta+\omega\tau)}$ to some power, $\pm p$, where $p = j-k$ for terms with coefficient $d_{jkl}$ and $p = j-k-1$ for coefficients $c_{jkl}$. Under the co-ordinate transformation (3.15), all these terms lead to integrals of the form (3.10) with $K = p\omega/\alpha$, from which we note that the exponentially biggest contributions come from $p = \pm 1$. We refer to all such contributions to $I_u^{(3)}$ as $I_{u1}^{(3)}$. Hence we have

$$\begin{aligned} I_{u1}^{(3)} = 2\frac{(\alpha+1)^{1/\alpha}}{\alpha}\sqrt{\mu}^{3+2/\alpha}\mathrm{Re}\Bigg\{ \int_{-\infty}^{\infty} d\tau \left[c_{003}s^3 + (\alpha+1)c_{111}s\right] \frac{e^{-i\theta}e^{-\frac{i\omega\tau}{\alpha\sqrt{\mu}}}}{[\cosh(\tau)]^{4+2/\alpha}} + \\ \left[(\alpha+1)c_{201}s + 2(\alpha+1)^{5/2}d_{210}s + 2(\alpha+1)^{3/2}d_{102}s^3\right] \frac{e^{i\theta}e^{\frac{i\omega\tau}{\alpha\sqrt{\mu}}}}{[\cosh(\tau)]^{4+2/\alpha}} \Bigg\}, \end{aligned}$$

where $s = \sinh\tau$ and we have reduced the number of terms using the relation (2.4). Using (3.10) on each term, we obtain

$$I_{u1}^{(3)} = 4\pi \frac{(\alpha+1)^{1/\alpha}}{\alpha\Gamma(4+2/\alpha)} \left(\frac{\omega}{\alpha}\right)^{2/\alpha} \left(K_r^{(3)}\cos\theta + K_i^{(3)}\sin\theta\right) e^{-\frac{\omega\pi}{2\alpha\sqrt{\mu}}}, \tag{3.18}$$

$$:= \gamma^{(3)}(\theta) e^{-\frac{\omega\pi}{2\alpha\sqrt{\mu}}}, \tag{3.19}$$

where

$$K_r^{(3)} = \left(\frac{\omega}{\alpha}\right)^3 \mathrm{Im}\left[-2(\alpha+1)^{5/2}d_{210} + 2(\alpha+1)^{3/2}d_{102} + (\alpha+1)(c_{111}-c_{201}) - c_{003}\right],$$

$$K_i^{(3)} = \left(\frac{\omega}{\alpha}\right)^3 \mathrm{Re}\left[-2(\alpha+1)^{5/2}d_{210} + 2(\alpha+1)^{3/2}d_{102} - (\alpha+1)(c_{201}+c_{111}) + c_{003}\right].$$

Thus we have

$$I_u^{(3)} = I_{u0}^{(3)} + I_{u1}^{(3)} + O\left(e^{-\frac{\omega\pi}{\alpha\sqrt{\mu}}}\right), \tag{3.20}$$

where $I_{u0}^{(3)}$ is given by (3.16) (also computed in [7]), and $I_{u1}^{(3)}$ is given by (3.19), which we have calculated explicitly here for the first time.

### *3.3 Intersections of manifolds*

Now that we have expressions for the stable and unstable manifolds of $P_+$ in the limit of small $\mu$, we find homoclinic connections to $P_+$ by locating intersections of these manifolds in a neighbourhood of $P_-$. As in [7, Sec. 3.6], we define a cylinder $U$ surrounding $P_-$ with surfaces $\Sigma^{\pm}$, defined by:

$$\Sigma^+ \,:\, z - z_- = \Delta$$

$$\Sigma^- \,:\, |q - q_-| = \Delta$$

where

$$\Delta = \delta\sqrt{\mu}$$

for some $\mu$-independent constant $\delta \ll 1$. See Fig. 3. We define local coordinates $(\hat{q}, \hat{z})$ within $U$ as follows:

$$q = q_- + \hat{q}, \qquad z = z_- + \hat{z}.$$

We shall seek intersections of $W^s(P_+)$ and $W^u(P_+)$ on $\Sigma^-$.

To find $W^s(P_+) \cap \Sigma^-$ we use the first-order approximation for $W^s(P_+)$ to locate the point $W^s(P_+) \cap \Sigma^+$, then use the vector field inside $U$ to find the preimage on $\Sigma^-$ of this point, i.e., $W^s(P_+) \cap \Sigma^-$. Now by standard estimates (see [17, Lemma 13.5]), the vector field within $U$ can be estimated by its linear part plus an error term

$$\hat{q}(t) = Ae^{i\omega t - \alpha\sqrt{\mu}t} + O\left(e^{-J\sqrt{\mu}t}\right), \tag{3.21}$$

$$\hat{z}(t) = Be^{2\sqrt{\mu}t} + O\left(e^{-(K-2)\sqrt{\mu}t}\right), \tag{3.22}$$

for some initial conditions $q(0) = A$ and $z(0) = B$, and constants $J > \alpha$ and $K > 2$. (There is a slight abuse of notation here; actually the error terms are $o(e^{-\tilde{J}\sqrt{\mu}t})$ and $o(e^{-(\tilde{K}-2)\sqrt{\mu}t})$ for any $\alpha < \tilde{J} < \min(\alpha+2, 2\alpha)$ and $2 < \tilde{K} < \min(\alpha+2, 4)$).

Using expressions (2.9), (2.10), (3.1)-(3.4), we find $T_+$ such that $z_s(T_+) = \Delta - \sqrt{\mu}$:

$$T_+ = -\frac{1}{2\sqrt{\mu}} \ln\left(\frac{2\sqrt{\mu}}{\Delta}\right), \tag{3.23}$$

and correspondingly,

$$q_s(T_+) = q_- - \frac{I_s^{(3)}}{2^\alpha}\left(\frac{2\sqrt{\mu}}{\Delta}\right)^{\frac{\alpha}{2}-\frac{i\omega}{2\sqrt{\mu}}}.$$

Matching the local and global coordinates for $W^s(P_+) \cap \Sigma^+$ (i.e., finding $A$ and $B$ such that $z_s(T_+) = \hat{z}_s(T_+), q_s(T_+) = \hat{q}_s(T_+)$) yields

$$A = -\frac{I_s^{(3)}}{2^\alpha},\ B = 2\sqrt{\mu}.$$

Using the linearised equations inside $U$, we find the intersection $W^s(P_+) \cap \Sigma^-$ occurs at time $T = T_+ + T_u$ where $T_u$ is determined by solving $|\hat{q}_s| = \Delta$:

$$T_u = \frac{1}{\alpha\sqrt{\mu}} \ln\left(\frac{|A|}{\Delta}\right).$$

Using (3.21), (3.22) and this expression for $T_u$, we obtain the leading-order expressions for the coordinates of $W^s(P_+) \cap \Sigma_-$:

$$\hat{q}_s = \frac{A}{|A|}\Delta \exp\left(i\frac{\omega}{\alpha\sqrt{\mu}} \ln\frac{|A|}{\Delta}\right) + O\left(\frac{|A|}{\Delta}\right)^{\frac{J-\alpha}{\alpha}} \tag{3.24}$$

$$\hat{z}_s = 2\sqrt{\mu}\left(\frac{|A|}{\Delta}\right)^{2/\alpha} + O\left(\frac{|A|}{\Delta}\right)^{\frac{K}{\alpha}}, \tag{3.25}$$

where $A$ was given above.

In contrast, $W^u(P_+) \cap \Sigma^-$ is a curve parametrised by $\theta$. Its leading-order expression follows from solving (2.11) for $T_-$, the positive time at which $|q| = \Delta$ then substituting this time into (3.6) and (3.7). Specifically, it is found that

$$T_- \approx \frac{1}{\alpha\sqrt{\mu}} \ln\left(\frac{2\sqrt{\mu(\alpha+1)}}{\Delta}\right)$$

from which it follows that

$$\hat{q}_u(\theta) = \Delta e^{i\theta} \exp\left(i\frac{\omega}{\alpha\sqrt{\mu}} \ln\left(\frac{2\sqrt{\mu}(1+\alpha)^{1/2}}{\Delta}\right)\right), \tag{3.26}$$

$$\hat{z}_u(\theta) = -\frac{I_u^{(3)}(\theta) + \lambda I_\lambda}{2\sqrt{\mu}(1+\alpha)\Delta^{2/\alpha}}. \tag{3.27}$$

In deriving this expression for $\hat{q}_u(\theta)$ we use the previously derived asymptotic behaviour of $I_u^{(3)}$ (3.16)-(3.20) and $I_\lambda$ (3.12) and assume $\lambda = o(\sqrt{\mu})$. This last assumption is justified by our subsequent calculation that for $\lambda, \mu$ near zero, the homoclinic bifurcations of interest occur in an exponentially thin wedge centred on a curve $\lambda = \text{constant} \times \mu + O(\mu^2)$.

In what follows it will be crucial how each of these intersections scale as $\mu \to 0$. Consider first the one-dimensional manifold. The argument of $A$ is

$$\arg(A) = \arg(I_s^{(3)}) + \pi$$

which is independent of $\mu$ since from (3.13) $\arg(I_s^{(3)})$ is independent of $\mu$. Hence from (3.24), after substitution of $I_s$ from (3.13), and writing $q = q_- + \Delta e^{i\hat{\phi}}$ for $q \in \Sigma^-$, the $\hat{\phi}$ co-ordinate of $W^s(P_+) \cap \Sigma^-$ is

$$\begin{aligned}
\hat{\phi}_s &= \arg(A) + \frac{\omega}{\alpha\sqrt{\mu}} \ln\left(\frac{|A|}{\Delta}\right) + O\left(\frac{1}{\Delta}\left(\frac{|A|}{\Delta}\right)^{\frac{J-\alpha}{\alpha}}\right) \\
&= \arg(A) + \left(\frac{\omega}{\alpha\sqrt{\mu}}\right) \ln\left(\frac{1}{\delta\sqrt{\mu}} \frac{2\pi\mu|c_{003}|}{2^\alpha \Gamma(3+\alpha)} \left(\frac{\omega}{\sqrt{\mu}}\right)^{2+\alpha} \left(\frac{2}{\delta}\right)^{\alpha/2} e^{-\frac{\pi\omega}{2\sqrt{\mu}}}\right) + o(1) \\
&= -\frac{\pi}{2}\frac{\omega^2}{\alpha\mu} + O\left(\frac{1}{\sqrt{\mu}}\right),
\end{aligned} \tag{3.28}$$

which is proportional to $1/\mu$ as $\mu \to 0$. Note that the $o(1)$ term comes about since $J > \alpha$ and $|A|$ is exponentially small.

The $z$–coordinate of $W^s(P_+) \cap \Sigma^-$, $\hat{z}_s$ given by (3.25), can be simplified to read

$$\begin{aligned}
\hat{z}_s &= \frac{\sqrt{\mu}}{2(\delta\sqrt{\mu})^{2/\alpha}} \left(|I_s^{(3)}|^{2/\alpha} + O\left(\left(\frac{1}{\sqrt{\mu}}|I_s^{(3)}|\right)^{K/\alpha}\right)\right) \\
&= \frac{\sqrt{\mu}}{2(\delta\sqrt{\mu})^{2/\alpha}} \left(\frac{2\pi\mu|c_{003}|}{\Gamma(3+\alpha)}\right)^{2/\alpha} \left(\frac{\omega}{\sqrt{\mu}}\right)^{2(2+\alpha)/\alpha} e^{\frac{-\omega\pi}{\alpha\sqrt{\mu}}} + \text{h.o.t.} \\
&:= k_s^{(3)} \sqrt{\mu}^{-(2+\alpha)/\alpha} e^{\frac{-\omega\pi}{\alpha\sqrt{\mu}}} + \text{h.o.t.},
\end{aligned} \tag{3.29}$$

where $k_s^{(3)}$ is independent of $\mu$ and the higher-order terms are asymptotically smaller since $K > 2$.

Consider next the two-dimensional manifold. From (3.26) we have that

$$\hat{\phi}_u = \theta + \frac{\omega}{\alpha\sqrt{\mu}} \ln\left(\frac{2\sqrt{\mu}(1+\alpha)^{1/2}}{\Delta}\right), \tag{3.30}$$

which is proportional to $1/\sqrt{\mu}$ as $\mu \to 0$. The $z$-component $\hat{z}_u$ is given by (3.27) and can be written as

$$\begin{aligned} \hat{z}_u(\theta) = -\frac{I^{(3)}_{u0} + \lambda I_\lambda}{2\sqrt{\mu}(1+\alpha)\Delta^{2/\alpha}} \quad &+ \quad \frac{I^{(3)}_{u1}(\theta)}{2\sqrt{\mu}(1+\alpha)\Delta^{2/\alpha}} \\ := \qquad \sigma^{(3)} \quad &+ \quad \kappa^{(3)}(\theta), \end{aligned}$$

where $\sigma^{(3)}$ contains the algebraic in $\mu$ terms and $\kappa^{(3)}$ contains the terms which, according to (3.18) are proportional to $\exp[-\pi\omega/(2\alpha\sqrt{\mu})]$. Specifically, from (3.12) and (3.16) we have, to lowest order in $\sqrt{\mu}$, that

$$\sigma^{(3)} = -\frac{2\lambda + \mu K^{(3)}_0}{2(1+\alpha)^{1-1/\alpha}\delta^{2/\alpha}} \frac{\sqrt{\pi}\Gamma(2+1/\alpha)}{\Gamma(3/2+1/\alpha)}$$

and from (3.18)

$$\kappa^{(3)} = \frac{\gamma^{(3)}(\theta) e^{-\frac{\omega\pi}{2\alpha\sqrt{\mu}}}}{2\sqrt{\mu}^{1+2/\alpha}(1+\alpha)\delta^{2/\alpha}}.$$

Now the curve in the $(\lambda, \mu)$-plane defined by $\sigma^{(3)} = 0$ defines the parameter values for which the two-dimensional unstable manifold $W^u(P^+)$ returns along the two-dimensional stable manifold of $W^s(P^-)$, up to exponentially small terms. Using (3.17) we see that this curve is given explicitly by

$$\begin{aligned} \lambda = h^{(3)}(\mu) := -\frac{\mu}{2(3\alpha+2)} \left[2\alpha \mathrm{Re}\, c_{102} + 4(\alpha+1)^2 \mathrm{Re}\, c_{210} + 3\alpha^2 d_{003}\right. \\ \left. + 2\alpha(\alpha+1) d_{111}\right]. \end{aligned} \tag{3.31}$$

In fact, this curve is the linear in $\mu$ approximation to a lot of different bifurcation events, which occur exponentially nearby in $\mu$. These include a pair of heteroclinic tangencies between the two two-dimensional manifolds, and the inherent Smale horseshoe dynamics that results. We shall refer to the curve $\lambda = h^{(3)}(\mu)$ as the *homoclinic axis*.

Note from the above asymptotic estimates that the beyond-algebraic-in-$\mu$ term in the $z$-component of the two-dimensional manifold is asymptotically larger than the $z$-component of the one-dimensional manifold given by (3.29), although both are exponentially small in $\mu$. Also, the phase $\hat{\phi}_u$ of $W^u(P_+) \cap \Sigma^-$,

given by (3.30), for fixed $\theta$ varies asymptotically slower with $\mu$ than that of $W^s(P_+) \cap \Sigma^-$ given by (3.28). It will be helpful then in what follows to make a $\mu$-dependent co-ordinate transformation that renders the two-dimensional manifold stationary as $\mu$ varies. Then we can consider the locus of the one-dimensional manifold as a function of $\mu$ and consider its intersection with the two-dimensional manifold parametrised by $\theta$ and $\lambda$. To this end we define

$$\tilde{z} = \frac{\hat{z}}{\kappa^{(3)}(\theta^{(3)}_{max})}, \quad \tilde{\phi} = \hat{\phi} - \theta^{(3)}_{max} - \frac{\omega}{\alpha\sqrt{\mu}} \ln\left(\frac{2\sqrt{\mu}(1+\alpha)^{1/\alpha}}{\Delta}\right), \tag{3.32}$$

where $\theta^{(3)}_{max}$ is the $\theta$-value leading to a positive maximum of $I^{(3)}_{u1}(\theta)$. Specifically, from (3.18) we have

$$\theta^{(3)}_{max} = \arctan(K^{(3)}_i/K^{(3)}_r) + \frac{1}{2}(1 - \mathrm{sign}K^{(3)}_r)\pi. \tag{3.33}$$

Now, after applying the co-ordinate transformation the unstable manifold becomes simply

$$\tilde{z}_u(\theta) = \tilde{\sigma} + \cos(\theta - \theta^{(3)}_{max}), \qquad \tilde{\phi}_u(\theta) = \theta - \theta^{(3)}_{max},$$

where

$$\tilde{\sigma} = \frac{\sigma^{(3)}}{\kappa^{(3)}(\theta^{(3)}_{max})}.$$

The stable manifold $W^s(P^+) \cap \Sigma^-$, using (3.28) and (3.29), becomes

$$\begin{aligned}
\tilde{z}_s &= \frac{k^{(3)}_s \mu^{-(2+\alpha)/\alpha}}{\kappa^{(3)}(\theta^{(3)}_{max})} e^{\frac{-\omega\pi}{\alpha\sqrt{\mu}}} \quad = \frac{2k^{(3)}_s(1+\alpha)\delta^{2/\alpha}}{\gamma^{(3)}(\theta^{(3)}_{max})} e^{-\frac{\omega\pi}{2\alpha\sqrt{\mu}}} \\
&:= \tilde{k}^{(3)}_s e^{-\frac{\pi\omega}{2\alpha\sqrt{\mu}}}, \\
\tilde{\phi}_s &= -\frac{\pi}{2}\frac{\omega^2}{\alpha\mu} + o\left(\frac{1}{\mu}\right).
\end{aligned}$$

As anticipated, in the new co-ordinate system $W^u(P_+) \cap \Sigma^-$ is independent of $\mu$ but is parametrised by $\theta$ and moves up and down with $\tilde{\sigma}$. By contrast, in the new coordinates, $W^s(P_+)(\theta) \cap \Sigma^-$ varies with $\mu$, sweeping out a curve in the $(\tilde{z}, \tilde{\phi})$-plane as shown in Fig. 4. Thus, to locate the homoclinic bifurcation involving $P_+$, we fix $\tilde{\sigma}$, thus fixing $W^u(P_+) \cap \Sigma^-$ in the $(\tilde{z}, \tilde{\phi})$-plane, and find a value of $\mu$ for which the locus of $W^s(P_+)(\theta) \cap \Sigma^-$ intersects $W^u(P_+) \cap \Sigma^-$. In Fig. 4 we show schematically the relative positions of $W^s(P_+)(\theta) \cap \Sigma^-$ and $W^u(P_+) \cap \Sigma^-$ for three different values of $\tilde{\sigma}$.

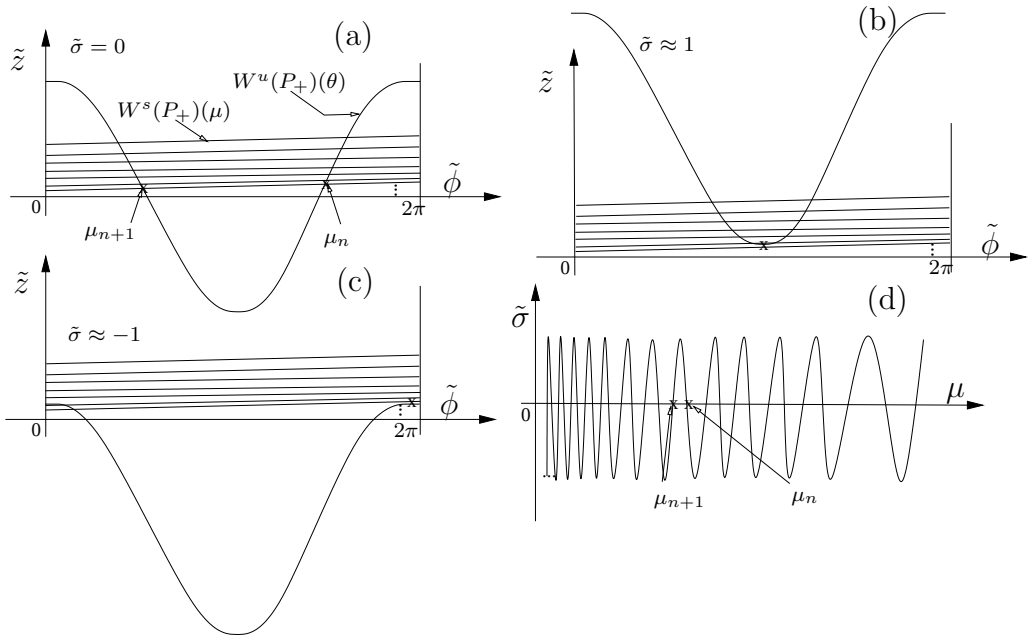


Fig. 4. The construction of the wiggly curve of homoclinic orbits to $P_+$. (a)–(c) Intersections between $W^u(P^+)$ and $W^s(P+)$ in the rescaled $(\tilde{\phi}, \tilde{z})$–co-ordinates of $\Sigma^-$ for three different $\tilde{\sigma}$-values. $W^u(P^+) \cap \Sigma^-$ is independent of $\mu$ while $W^s(P+) \cap \Sigma^-$ sweeps out a curve in the $(\tilde{z}, \tilde{\phi})$-plane as $\mu$ is varied. For each fixed $\tilde{\sigma}$ intersections between $W^u(P^+)$ and $W^s(P+)$ occur at isolated values of $\mu$; a subset of such $\mu$-values are shown in each case. (d) Locus of intersection points in the $(\tilde{\sigma}, \mu)$ parameter plane.

Note from this construction that if $\tilde{\sigma} = 0$ there are infinitely many $\mu$-values at which there are homoclinic connections (Fig. 4(a)). Consider one such $\mu$-value $\mu = \mu_n$, say, corresponding to $\tilde{\phi} = \tilde{\phi}_n$. Upon increasing $\tilde{\sigma}$, such a point of intersection is destroyed when (Fig. 4(b))

$$\tilde{\phi} \approx \pi, \quad \tilde{z}_u = \tilde{\sigma} - 1 = \tilde{z}_s + O\left(e^{-\frac{\pi\omega}{2\alpha\sqrt{\mu_n}}}\right).$$

That is, undoing the co-ordinate transformation (3.32),

$$\sigma^{(3)} = \kappa^{(3)}(\theta^{(3)}_{max}) + O\left(e^{-\frac{\pi\omega}{\alpha\sqrt{\mu_n}}}\right).$$

Similarly, upon decreasing $\tilde{\sigma}$ the homoclinic orbit is destroyed when

$$\sigma^{(3)} = -\kappa^{(3)}(\theta^{(3)}_{max}) + \text{h.o.t.}$$

From the definition of $\sigma^{(3)}$ and $\kappa^{(3)}$, these expressions give the envelope of the wiggly homoclinic bifurcation curve in the original ($\lambda$, $\mu$) co-ordinates. Specifically the homoclinic locus is given by the homoclinic axis plus an oscillatory function that sits between the two curves defined by

$$\lambda = h^{(3)}(\mu) \pm \frac{\Gamma(3/2 + 1/\alpha)}{2\sqrt{\pi}\Gamma(2 + 1/\alpha)} \frac{1}{(1+\alpha)^{\frac{1}{\alpha}}\sqrt{\mu}^{1+2/\alpha}} \gamma^{(3)}(\theta^{(3)}_{max}) e^{-\frac{\pi\omega}{2\alpha\sqrt{\mu}}}, \quad (3.34)$$

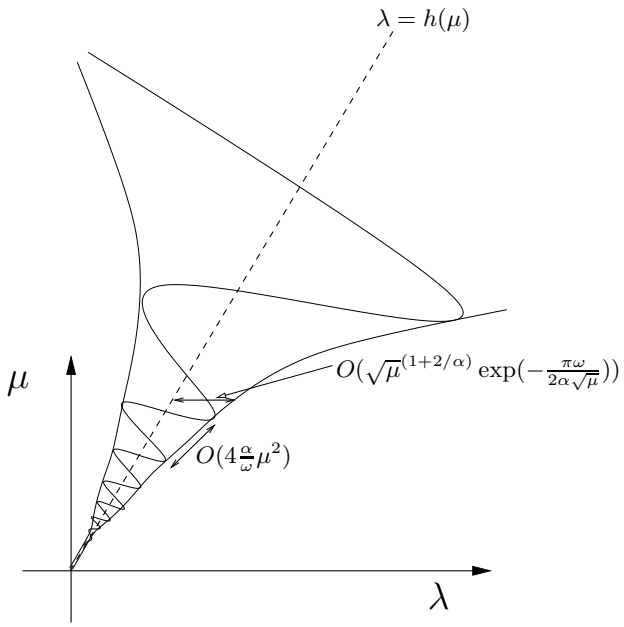


Fig. 5. The asymptotics of the wiggly curve of homoclinic orbits in the original $\mu, \lambda$ parameter plane.

where $h^{(3)}$ is defined by (3.31) and $\gamma^{(3)}$ by (3.19). See Fig. 5.

We can also obtain the frequency of the wiggly curve within this envelope. To do this note that the phases of two alternate $\mu$-values, $\mu_n$ and $\mu_{n+1}$, corresponding to successive intersections between the stable and unstable manifolds of $P_+$ at $\tilde{\sigma} = 0$, satisfy

$$\tilde{\phi}(\mu_n) \approx \tilde{\phi}(\mu_{n+1}) + \pi,$$

which implies that

$$-\frac{\pi}{2}\frac{\omega^2}{\alpha\mu_n} = -\frac{\pi}{2}\frac{\omega^2}{\alpha\mu_{n+1}} + \pi + \text{h.o.t.} \tag{3.35}$$

Hence

$$\mu_n - \mu_{n+1} = 2\frac{\alpha}{\omega^2}\mu_n\mu_{n+1} + \text{h.o.t} = 2\frac{\alpha}{\omega^2}\mu_n^2 + \text{h.o.t}, \tag{3.36}$$

so that the distance between alternate turning points on the wiggly homoclinic bifurcation curve as illustrated in Fig. 5 goes like $\frac{4\alpha\mu^2}{\omega^2}$ as $\mu \to 0$.

### *3.4 Effect of higher-order terms*

So far, we have calculated the loci of the homoclinic bifurcations of $P_+$ for the case that the perturbations $F$ and $G$ in (2.1), (2.2) contain cubic terms

only. We now modify our calculations to allow for terms of arbitrary order $\geq 3$ in the Taylor series for $F$ and $G$ (2.3). The effect that this has on the above analysis is simply to replace $I_{s,u}^{(3)}$ by $I_{s,u}$ in all our calculations. We do however need to calculate new asymptotic estimates for the general case $I_{s,u} = \sum_{n\geq 3} I_{s,u}^{(n)}$. One might naively think that terms $I_{s,u}^{(n)}$ for $n > 3$ contribute to these integrals at lower order in $\sqrt{\mu}$ than for $n = 3$. We shall show that this is not the case for the exponentially small integrals $I_s$ and $I_{u1}$, for which all nonlinear terms in $F$ and $G$ contribute at the same order. However, we can show that the contribution from this infinite number of terms is summable, because of the assumption that $F$ and $G$ are analytic. Similarly, the algebraic-in-$\mu$ integral $I_{u0}$ can be shown to be a convergent power series in $\mu$, and hence the homoclinic axis $\lambda = h_u(\mu)$ is an analytic curve.

Consider first the integral $I_s$. By definition (3.5) the contribution from $n^{th}$-order terms in the Taylor expansion is

$$I_s^{(n)} = \sqrt{\mu}^{n-1} c_{00n} \int_{-\infty}^{\infty} d\tau \frac{[\sinh(\tau)]^n}{[\cosh(\tau)]^{n+\alpha}} e^{-i\frac{\omega}{\sqrt{\mu}}\tau},$$

which, using (3.10), is

$$\sim (-1)^n \frac{2\pi (i)^n c_{00n} \omega^{n-1+\alpha}}{n! \sqrt{\mu}^{\alpha} \Gamma(\alpha)} e^{-\frac{\pi\omega}{2\sqrt{\mu}}}, \quad \text{as} \quad \mu \to 0.$$

Hence

$$I_s \sim \frac{2\pi\omega^{\alpha}}{\sqrt{\mu}^{\alpha}\Gamma(\alpha)} e^{-\frac{\pi\omega}{2\sqrt{\mu}}} \sum_{n}^{\infty} (-i)^n c_{00n} \frac{\omega^{n-1}}{n!}. \tag{3.37}$$

Now, the constants $c_{00n}$ are coefficients of a convergent Taylor series with a finite radius of convergence $R$, say. Hence $|c_{00(n+1)}|/|c_{00n}| \leq R$ for $n$ sufficiently large, and hence the sum in (3.37) converges by the ratio test. Thus $I_s$ has precisely the same asymptotic form as $I_s^{(3)}$, i.e. $I_s \propto \sqrt{\mu}^{-\alpha} \exp(-\frac{\pi\omega}{2\sqrt{\mu}})$, but with a different constant of proportionality.

Consider next the algebraic-in-$\mu$ portion of $I_u$, i.e., $I_{u0}$. Contributions to this come from terms in $F$ and $G$ with coefficients

$$c_{jkl} \quad \text{with} \quad j = k + 1, \qquad d_{jkl} \quad \text{with} \quad j = k, \tag{3.38}$$

Observe in the case that $n = j + k + l$ is even that all terms of the form (3.38) lead to terms in the expression for $I_u$ that are odd in $z_{u0}$. Since $|q_{u0}|$ is an even function of $t$ and $z_{u0}$ is an odd function of $t$, we are faced with integrals from $-\infty$ to $\infty$ of a sum of odd functions. Hence $I_{u0}^{(n)} = 0$ for $n$ even.

So the only contributions to $I_{u0}$ come from odd $n$. Simple book-keeping shows the $\mu$-dependence of each of the terms

$$I_{u0}^{(n)} = \sqrt{\pi}(1+\alpha)^{1/\alpha}\frac{\Gamma(2+1/\alpha)}{\Gamma(3/2+1/\alpha)}K_0^{(n)}\sqrt{\mu}^{n+2/\alpha}, \quad n \text{ odd}, \tag{3.39}$$

for certain $\alpha$-dependent constants $K_0^{(n)}$. The evaluation of $K_0^{(3)}$ was given in (3.17), and a similar calculation reveals

$$\begin{aligned} K_0^{(5)} = \frac{1}{(5\alpha+2)(3\alpha+2)}\Big[&6\alpha^2 \mathrm{Re}\, c_{104} + 4\alpha(1+\alpha)^2 \mathrm{Re}\, c_{212} \\ &+8(2\alpha+1)(1+\alpha)^3 \mathrm{Re}\, c_{320} + 15\alpha^3 d_{005} + \\ &6\alpha^2(1+\alpha)d_{113} + 4\alpha(1+\alpha)^3 d_{221}\Big]. \end{aligned} \tag{3.40}$$

This leads to a redefinition of $\sigma$:

$$\sigma = \sum_{m=1}^{\infty}\sigma^{(2m+1)} = -\frac{2\lambda + \sum_{m=1}^{\infty}\mu^m K_0^{(2m+1)}}{2(1+\alpha)^{1-1/\alpha}\delta^{2/\alpha}}\frac{\sqrt{\pi}\Gamma(2+1/\alpha)}{\Gamma(3/2+1/\alpha)},$$

and the homoclinic axis

$$\lambda = h(\mu) = \sum_{m=1}^{\infty} h^{(2m+1)}(\mu) = -\frac{1}{2}\sum_{m=1}^{\infty}\mu^m K_0^{(2m+1)}. \tag{3.41}$$

This then is an asymptotic expansion in $\mu$ for the homoclinic axis, where each coefficient is independent of $\mu$. In fact, our assumption about the analyticity of the system means that this series actually converges, for sufficiently small $\mu$, as the argument in Appendix B shows. Hence the homoclinic axis is indeed a smooth curve as depicted in Fig. 4.

Finally, consider general terms in $I_{u1}$, which come from terms in the integrand of $I_u$ that are proportional to $\exp(\pm i(\theta+\omega\tau))$. Such terms come from coefficients in the Taylor expansion of $F$ and $G$ within the set $S_1$ defined by

$$S_1 := \{c_{jkl} \text{ with } j = k \text{ or } j = k+2, \quad d_{jkl} \text{ with } j = k \pm 1\}. \tag{3.42}$$

Reasoning similar to that leading to (3.18) then shows that

$$I_{u1}^{(n)} \sim 4\pi\frac{(\alpha+1)^{1/\alpha}}{\alpha\Gamma(n+1+2/\alpha)}\left(\frac{\omega}{\alpha}\right)^{n+2/\alpha}(C_r^{(n)}\cos\theta + C_i^{(n)}\sin\theta)e^{-\frac{\pi\omega}{2\alpha\sqrt{\mu}}}. \tag{3.43}$$

Here, each coefficient $C_{r,i}^{(n)}$ is a function of $\alpha$ only and is sum of at most $4n$ terms, corresponding to (3.42) with $j+k+l = n$, where each term has

magnitude $|c_{jkl}|$ or $|d_{jkl}|$ multiplied by a factor $(\sqrt{1+\alpha})^q$ for some $0 \le q \le (2+n)$. Hence we can bound

$$|C_{r,i}^{(n)}| \le 4n(1+\alpha)^{1+n/2} d_n \qquad \text{where} \quad d_n = \max_{j+k+l=n} \{|c_{jlk}|, |d_{jkl}| \in S_1\} . \quad (3.44)$$

By definition of the $\Gamma$ function, we can write

$$I_{u1} \sim 4\pi \frac{(\alpha+1)^{1/\alpha}}{\alpha \Gamma(2/\alpha)} \left(\frac{\omega}{\alpha}\right)^{2/\alpha} e^{-\frac{\pi\omega}{2\alpha\sqrt{\mu}}} \sum_{n=3}^{\infty} (K_r^{(n)} \cos\theta + K_i^{(n)} \sin\theta)$$

where

$$\left|K_{r,i}^{(n)}\right| = \frac{1}{(n+2/\alpha)(n-1+2/\alpha)\dots(2/\alpha)} \left(\frac{\omega}{\alpha}\right)^n \left|C_{r,i}^{(n)}\right| \le \frac{d_n}{n!} \left(\frac{\omega}{\alpha}\right)^n 4n(1+\alpha)^{1+n/2}. \quad (3.45)$$

Now, $\{d_n\}_{n\ge 3}$ is a bounded sequence since the coefficients $c_{jkl}$ and $d_{jkl}$ are from a convergent Taylor series. Hence by the Dominated Convergence Theorem, (3.45) shows that the sequences $\{K_r^{(n)}\}_{n\ge 3}$ and $\{K_i^{(n)}\}_{n\ge 3}$ converge. Let their limits be respectively $K_r$ and $K_i$. Then we have

$$I_{u1} \sim 4\pi \frac{(\alpha+1)^{1/\alpha}}{\alpha \Gamma(2/\alpha)} \left(\frac{\omega}{\alpha}\right)^{2/\alpha} (K_r \cos\theta + K_i \sin\theta) e^{-\frac{\pi\omega}{2\alpha\sqrt{\mu}}} := \gamma(\theta) e^{-\frac{\pi\omega}{2\alpha\sqrt{\mu}}},$$

This has precisely the same form as the expression (3.18) with the bounded real constants $K_r^{(n)}$ and $K_i^{(n)}$ replaced by the bounded real constants $K_r$ and $K_i$.

In summary, we have shown in this section that with the inclusion of arbitrary terms rather than just cubic in the perturbation to the normal form, similar expressions apply for all the various asymptotic quantities needed in the analysis in Section 3.3 above. In fact, one simply needs to drop all superscripts (3), and the analysis of that section applies almost verbatim. The homoclinic axis, which was linear in $\mu$, becomes a general curve $\lambda = h(\mu)$, passing through $(\lambda, \mu) = (0, 0)$, for which $h^{(3)}$, given by (3.31), gives only its linear part. Its quadratic part is given by (3.41). The envelope of the homoclinic locus remains an exponentially thin wedge around the homoclinic axis (3.34), with the constant $\gamma^{(3)}(\theta_{max}^{(3)})$ replaced by $\gamma(\theta_{max})$ and where $\theta_{max}$ is defined by the removal of the superscript (3) in the formula (3.33). The asymptotic formulae (3.36) for the frequency of the oscillations of the locus within this wedge is entirely unaffected.

Note that the following transformation applied to the full perturbed dynamical system (2.1), (2.2)

$$z \mapsto -z, \quad t \mapsto -t, \quad (\omega, \lambda) \mapsto (-\omega, -\lambda), \tag{3.46}$$

$$c_{jkl} \mapsto -c_{jkl} \text{ iff } l \text{ even}, \quad d_{jkl} \mapsto -d_{jkl} \text{ iff } l \text{ odd}, \tag{3.47}$$

results in a new system in which the equilibrium $P_-$ is mapped to $P_+$ and *vice versa*. Now we can simply apply this transformation to the locus of homoclinic orbits to $P_+$ computed above and we obtain the locus of homoclinic orbits to $P_-$.

Consider first the homoclinic axis $\lambda = h(\mu)$ given by (3.41). By construction $h(\mu)$ is a sum of terms with coefficients

$$c_{jkl} \quad \text{with } j+k+l \text{ odd and } j = k+1; \text{ hence } l \text{ is even},$$

$$d_{jkl} \quad \text{with } j+k+l \text{ odd and } j = k; \text{ hence } l \text{ is odd}.$$

Note that all such terms change their sign under the transformation (3.46), (3.47). Hence, since $\lambda \to -\lambda$ under this transformation the curve $\lambda = h(\mu)$ is invariant under the transformation, and the homoclinic axis for homoclinic orbits to $P_-$ is the same as that for $P_+$.

Next we consider the wiggling within the exponentially thin wedge around the homoclinic axis. By construction the integral $I_s$ is formed of terms proportional to $c_{00l}$, so if we write $I_s^-$ for the transformation of $I_s$ under (3.46), (3.47) we find

$$I_s^- = I_s^{(3)} - I_s^{(4)} + I_s^{(5)} + \ldots = \sum_3^\infty (-1)^{n+1} I_s^{(n)}. \tag{3.48}$$

Similarly, $I_{u1}^{(n)}$ is determined by terms:

$$\begin{aligned} c_{jkl} \quad & \text{with } j+k+l = n \text{ and } j = k \text{ or } j = k+2; \text{ hence } l \text{ is even iff } n \text{ is even;} \\ d_{jkl} \quad & \text{with } j+k+l = n \text{ and } j = k \pm 1; \text{ hence } l \text{ is odd iff } n \text{ is even.} \end{aligned} \tag{3.49}$$

So, we find that $I_{u1}^-$, the transformation of $I_{u1}$ under (3.46), (3.47), satisfies

$$I_{u1}^- = \sum_3^\infty (-1)^{n+1} I_{u1}^{(n)}.$$

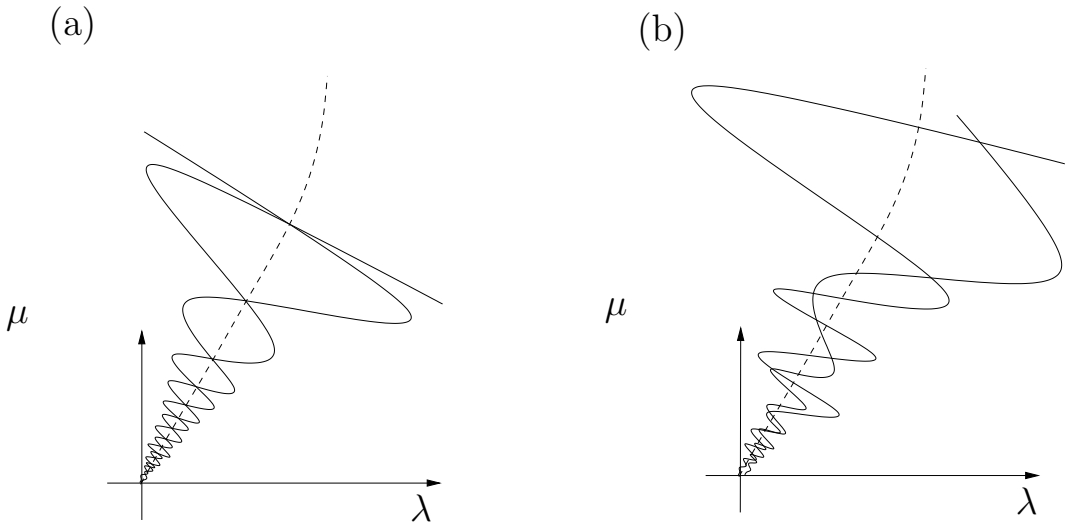


Fig. 6. Entwined wiggling of loci of homoclinic orbits to $P_+$ and $P_-$: (a) with just cubic perturbation terms; (b) with general perturbations.

Hence in the case of purely cubic perturbations, we find that $K_r^{(3)}$ and $K_i^{(3)}$ change sign under the transformation (3.46), (3.47), from which we deduce that

$$\theta_{max}^{(3)} \mapsto \theta_{max}^{(3)} - \pi, \quad \gamma^{(3)}(\theta_{max}^{(3)}) \mapsto \gamma^{(3)}(\theta_{max}^{(3)}). \tag{3.50}$$

Thus, in the case of purely cubic perturbations the locus of homoclinic orbits to $P_-$ is *precisely out of phase* with the locus of homoclinic orbits to $P_+$, but the curves lie inside the *same* exponentially thin wedge around the homoclinic axis. This agrees with the numerical results in [12] where only cubic perturbations were used. See Fig. 6(a).

However, in the presence of arbitrary perturbations $F$ and $G$, all the coefficients of $I_s$ and $I_{u1}$ generically change under the transformation (3.46), (3.47), including $\theta_{max}$ and $\gamma(\theta_{max})$. This means that although the curves of homoclinic bifurcations to $P_-$ and $P_+$ have the same asymptotics (i.e., in the limit $\mu \to 0$ the curves are tangent to the same line and have the same frequency of oscillation) the curves wiggle inside *different* exponentially thin wedges around the homoclinic axis, and the phases of the oscillations within these wedges are uncorrelated with one another.

## 4 Numerical results

In this section we compare our theoretical predictions with numerical studies on three systems with SNH instabilities of the appropriate type ($\alpha > 0$, $s =$

$-1$). In all cases we compute homoclinic curves as two parameters are varied using AUTO [5]. This is done by first following a branch of periodic orbits up to large period, well away from the SNH point, and then following orbits of fixed large period toward the SNH point.

### *4.1 Cubically perturbed normal form equations*

We first consider the equations

$$\dot{q} = (\lambda + 1.25i)q + 3zq + c_{111}z|q|^2 + c_{003}z^3, \tag{4.1}$$
$$\dot{z} = \mu - z^2 - |q|^2 - d_{003}z^3. \tag{4.2}$$

These arise as a special case of equations (2.1), (2.2), corresponding to the choice $\omega = 1.25$, $\alpha = 3$, $\beta = 0$, and with all terms in $F$ and $G$ vanishing except the cubic terms with coefficients $c_{111}$, $c_{003}$ and $d_{003}$. The choice

$$c_{111} = 0.4, \quad c_{003} = 0.05, \quad d_{003} = -0.4, \tag{4.3}$$

leads to precisely the equations studied in [11,12]. There, entwined wiggly curves of homoclinic bifurcations were found to emanate from the SNH instability at $(\lambda, \mu) = (0, 0)$. We have recomputed these curves here, with the results shown in Fig. 1. These results agree qualitatively with the predictions of Sec. 3.3; the homoclinic bifurcation curves appear to oscillate within a common envelope, with the two bifurcation curves having oscillations of similar frequency, but being precisely out of phase.

The numerical results also have reasonable quantitative agreement with our theoretical predictions, as demonstrated in Fig. 7. In constructing this figure, we calculated the $\mu$ values for turning points on each of the homoclinic bifurcation curves. From (3.36) we expect the change in $\mu$ between adjacent maxima (with respect to $\lambda$) on one of the homoclinic bifurcation curves to scale with $\mu$ as

$$\mu_n - \mu_{n+1} \sim \frac{4\alpha}{\omega^2}\mu_n^2 = 7.68\mu_n^2,$$

or

$$\sqrt{\mu_n - \mu_{n+1}} \sim 2.77\mu_n.$$

The $\mu$ values for adjacent minima have the same scaling. In Fig. 7(a) we plot the theoretical prediction $f(\mu) = 2.77\mu$ (solid line in the figure) and four data sets: $\sqrt{\mu_n - \mu_{n+1}}$ versus $\mu_n$ for successive maxima of one wiggly curve, then successive minima of that curve, and similarly successive maxima/minima of the other wiggly curve. We see that all the data sets lie close to the theoretical prediction even though our prediction is for asymptotically small $\mu$ and the

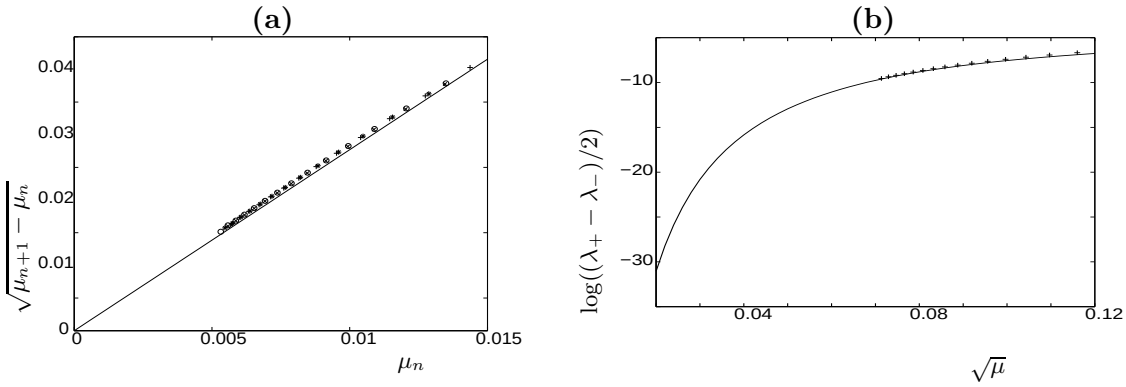


Fig. 7. Comparison of theory and numerics for the homoclinic bifurcations curves associated with the SNH point at $(\lambda, \mu) = (0, 0)$ in (4.1), (4.2) at parameter values (4.3). Panel (a) shows the data for the scaling of the frequency of the oscillations, plotting difference between successive maxima ('x' and '$*$') and minima ('$+$' and $\circ$) on the two homoclinic curves respectively. This is compared with the theoretical prediction (straight line). (b) Shows the exponential scaling of the envelope of the locus, by taking half the difference between the $\lambda$-values on the two out-of-phase curves at the maximum points of one of the loci, and plotting the $\mu$-dependence of this quantity on an appropriate scale. The solid line shows the theoretical prediction (4.4).

numerical results are for only moderately small $\mu$. Fig. 7(a) shows clearly the relationship between the phases of oscillation for the two wiggly curves; the data points corresponding to maxima of one curve lie almost on top of the data points corresponding to minima of the other curve, confirming that the wiggles are out of phase as predicted for the case of cubic perturbations of the normal form. This phase correspondence is not expected to hold in the case of arbitrary perturbation of the normal form, and an illustration of this situation will be seen in the next example.

The quantitative agreement between theory and numerics for this example is further illustrated by Fig. 7(b). Recall from (3.34) that the difference between the envelope of the homoclinic locus and the homoclinic axis is (to lowest order)

$$k(\alpha)\sqrt{\mu}^{-(1+2/\alpha)} \exp(-\pi\omega/2\alpha\sqrt{\mu})$$

where

$$k(\alpha) = \frac{\Gamma(3/2 + 1/\alpha)}{2\sqrt{\pi}\Gamma(2 + 1/\alpha)} \frac{1}{(1+\alpha)^{\frac{1}{\alpha}}} \gamma^{(3)}(\theta_{max})$$

where $\gamma^{(3)}(\theta_{max})$ was defined in (3.19).

For the values of the parameters used here, we have that $\theta_{max} = -\pi/2$ and hence $k(\alpha) = 0.00397$. Because the homoclinic loci in this example are out-of-phase, we can estimate the difference between the homoclinic axis and the envelope by half the difference between the $\lambda$ values on the homoclinic loci at the maximum points of one of the loci. Fig. 7(b) plots the logarithm of this

estimate versus $\sqrt{\mu}$; once again we get good fit between theory and numerics with the data lying remarkably close to the theoretically predicted curve

$$\log[(\lambda_1 - \lambda_2)/2] = \log(k(\alpha)) - (1 + 2/\alpha)\log(\sqrt{\mu}) - \pi\omega/(2\alpha\sqrt{\mu}) \quad (4.4)$$

despite the fact that $\sqrt{\mu} > 0.07$ for these data.

In summary, we find good qualitative and quantitative agreement between theory and numerics for this example of a cubic perturbation of the normal form, even though the theory is derived for asymptotically small $\mu$ but the numerics have only moderately small $\mu$.

### *4.2 A model for calcium wave propagation*

As part of a study of a model for intracellular calcium wave propagation, Sneyd et al. [20] numerically investigate the equations

$$c' = d, \quad (4.5)$$

$$d' = \frac{1}{25}\left[sd - 28\left(\frac{ph\phi_1}{\phi_1 p + \phi_{-1}}\right)^4 + \frac{1.2c^2}{0.0324 + c^2} - 0.2\right], \quad (4.6)$$

$$sh' = \phi_3(1 - h) - \left(\frac{\phi_1\phi_2 p}{\phi_1 p + \phi_{-1}}\right)h, \quad (4.7)$$

where

$$\phi_1(c) = \frac{100c}{6 + c},\ \phi_{-1}(c) = \frac{44}{50 + c},\ \phi_2(c) = \frac{26.5 + 20c}{50 + c},\ \phi_3(c) = \frac{1.6}{1.6 + c}.$$

In these equations, $c, d$ and $h$ are real variables while $p$ and $s$ are bifurcation parameters. See [20] for details of the derivation of the model and for the physiological significance of the variables and parameters. Sneyd et al. were particularly interested in the existence of homoclinic orbits in these equations; such orbits correspond to isolated travelling wave solutions in an underlying PDE model for calcium wave propagation. They located two SNH instabilities in their model (called LP1 and LP2 in [20]), one of which (LP2, at $(p, s) = (0.24594, 5.4177)$) is of the type of interest to us. They located a wiggly curve of homoclinic bifurcations, which they denoted branch C, emanating from LP2. Sim [19] investigated some aspects of this model further, and found a second wiggly curve of homoclinic bifurcations (branch D in [19]) coming out of LP2. Figure 8 shows the loci of branches C and D for values of the parameters $p$ and $s$ near LP2. A striking feature of this figure is that the two bifurcation curves do not look alike and in particular the frequencies of oscillation of the

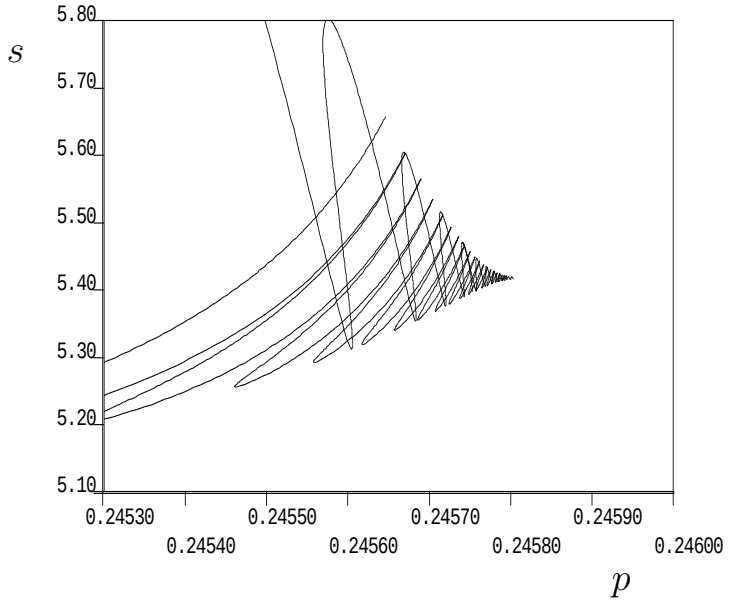


Fig. 8. Loci of homoclinic bifurcation curves near LP2 for (4.5)-(4.7).

two curves do not appear to be close, in contrast to our prediction that as LP2 is approached the frequencies of oscillation should become equal. However, we note from (3.35) and (3.28) that the rate of crossing of the homoclinic axis as $\mu \to 0$ goes like $1/\mu + O(1/\sqrt{\mu})$. The $O(1/\mu)$ term should be the same for both homoclinic loci, but the error term will in general depend on $I_u$ and $I_s$ and hence is different for the two different loci. Since the values of the parameters $p$ and $s$ at the parts of the homoclinic loci shown in Fig. 8 are still some way off their values at the SNH point, the effect of the $O(1/\sqrt{\mu})$ term may be quite large, leading to apparent discrepancies in the frequency of oscillation of the two homoclinic loci. In fact, if we zoom in on the homoclinic loci near the SNH point we do indeed find that, consistent with our predictions, the shapes of the two bifurcation curves and their frequencies of oscillation become more similar as LP2 is approached. We note that, although their phases are uncorrelated, the two wiggly curves approximately lie within a common envelope.

To make quantitative comparisons between theory and numerics for this example, it is necessary to do a normal form reduction near LP2. Application of the procedure in [13, Sec. 8.5] yields the unfolded normal form, truncated at quadratic order:

$$\dot{r} = (0.0400\hat{s} + 4.12352\hat{p})r + 0.9778rz, \tag{4.8}$$

$$\dot{\theta} = 0.1368 + 1.1858z, \tag{4.9}$$

$$\dot{z} = -2.4812\hat{p} - r^2 - z^2, \tag{4.10}$$

where we write $p = p_0 + \hat{p}$, $s = s_0 + \hat{s}$, and the SNH point is at $(p, s) = (p_0, s_0) \equiv (0.24594, 5.4177)$. We identify $\alpha = 0.9778$, $\omega = 0.1368$ by comparing equations

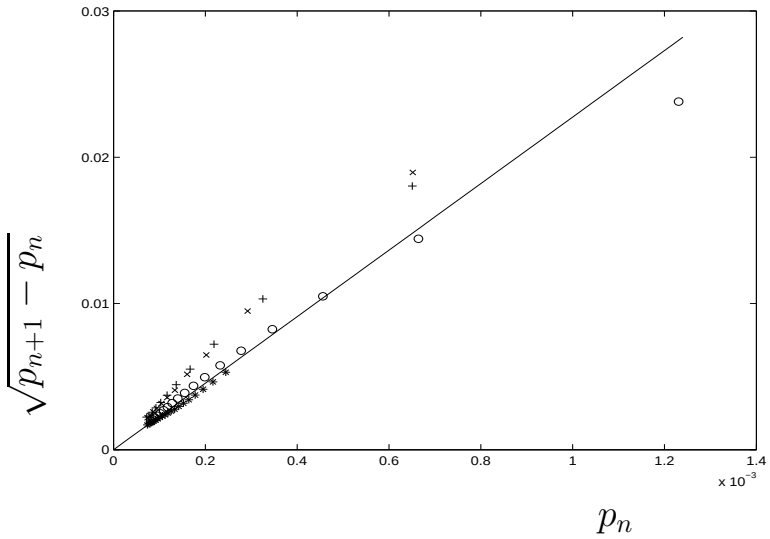


Fig. 9. Comparison of theory and numerics for the frequency of oscillation of the homoclinic bifurcations curves associated with the SNH point of the calcium wave model (4.5)–(4.7). The figure is drawn similarly to Fig. 7(a).

(4.8)-(4.10) with equations (2.5). Note that the removal of $\beta$ from this normal form will in general alter $\alpha$ (see (2.8)) but only at higher order. So, precisely at the singularity, $\alpha$ remains unaffected. Hence, our analysis predicts that the $p$ values for alternate turning points on each of branches C and D will, in the limit of $p \to p_0$ scale as

$$p_{n+1} - p_n \sim \frac{4\alpha}{\omega^2}(2.4812)(p_n - p_0)^2 = 518.6(p_n - p_0)^2$$

where $p_n$ is the $p$ value at the $n$-th maximum or minimum of the relevant homoclinic locus.

Fig. 9 shows a comparison between theory and numerics for the calcium wave model (4.5)–(4.7). In this figure, the solid line shows the theoretical prediction, and the four data sets (represented by 'x', '$*$', '+', and $\circ$ respectively) are derived from the $p$ and $s$ values of the turning points on the two homoclinic branches, just as described for the example in Sec. 4.1 which produced Fig. 7. Quantitative agreement between our theory and the numerics is evident in Fig. 9, with the fit improving as the SNH point is approached, as expected.

### *4.3 The 'other' Lorenz equations*

In [16], Shil'nikov, Nicolis and Nicolis perform a bifurcation analysis of the system of equations originally due to Lorenz [14]

$$\dot{X} = -Y^2 - Z^2 + \frac{1}{4}(F - X), \tag{4.11}$$

$$\dot{Y} = XY - 4XZ - Y + G, \tag{4.12}$$

$$\dot{Z} = 4XY + XZ - Z. \tag{4.13}$$

This system arises as a low-order truncation of a model for atmospheric circulation, where $X$ represents a globally averaged westerly current strength, and $Y$ and $Z$ the components of a generalised superimposed wave. The parameters $F$ and $G$ represent thermal forcings. The specific details of the atmospheric model do not concern us here. Instead we wish to focus on a SNH point that was identified in [16], from which were found to emanate two wiggly curves of saddle-focus homoclinic orbits one of which was shown to organise the creation of strange attractors. (Note that this mechanism is unlike the more famous Lorenz equations, where the theory of homoclinic explosions involving symmetric equilibria plays a key role.)

Specifically, the SNH occurs at $(F, G) \approx (1.6829, 1.6840)$. In Fig. 10 we have computed the two curves of homoclinic orbits that arise out of this point. Note that, as in the example in the previous section, the accumulation rate of oscillations does not appear to be the same for the two curves, at least on the scale used to draw the figure. Again we note that the homoclinic loci shown are still some way off the SNH point, and the $O(1/\sqrt{\mu})$ error term in our prediction may produce a discrepancy in the accumulation rates such as that observed. When translated into the co-ordinates plotted in Fig. 11, such an error term would give rise to a quadratic correction to the straight line that is the theoretical prediction as the SNH point is approached. The data plotted in Fig. 11 is indeed consistent with curves that become tangent to the straight line as $\mu \to 0$.

In computing the theoretical prediction in Fig. 11, we needed to derive the normal form for the SNH bifurcation. Again following the procedure in [13, Sec. 8.5] one finds the unfolded, truncated normal form to be:

$$\begin{aligned}
\dot{r} &= \lambda(F, G)r + 4.062rz, \\
\dot{\theta} &= 4.526 + 11.930z, \\
\dot{z} &= 0.3075(0.2626(F - F_0) - 0.1745(G - G_0)) - r^2 - z^2,
\end{aligned}$$

where the SNH bifurcation occurs at $(F, G) = (F_0, G_0) \equiv (1.6829, 1.6840)$, and where $\lambda(F, G)$ is some linear combination of the parameters $F$ and $G$. We identify $\alpha = 4.062$ and $\omega = 4.526$, and note that as in the previous example, rescaling to remove $\beta$ will not affect $\alpha$ at lowest order. Writing $\mu = 0.2626(F - F_0) - 0.1745(G - G_0)$, our analysis predicts that the $\mu$ values for alternate turning points on each of the homoclinic loci will, in the limit

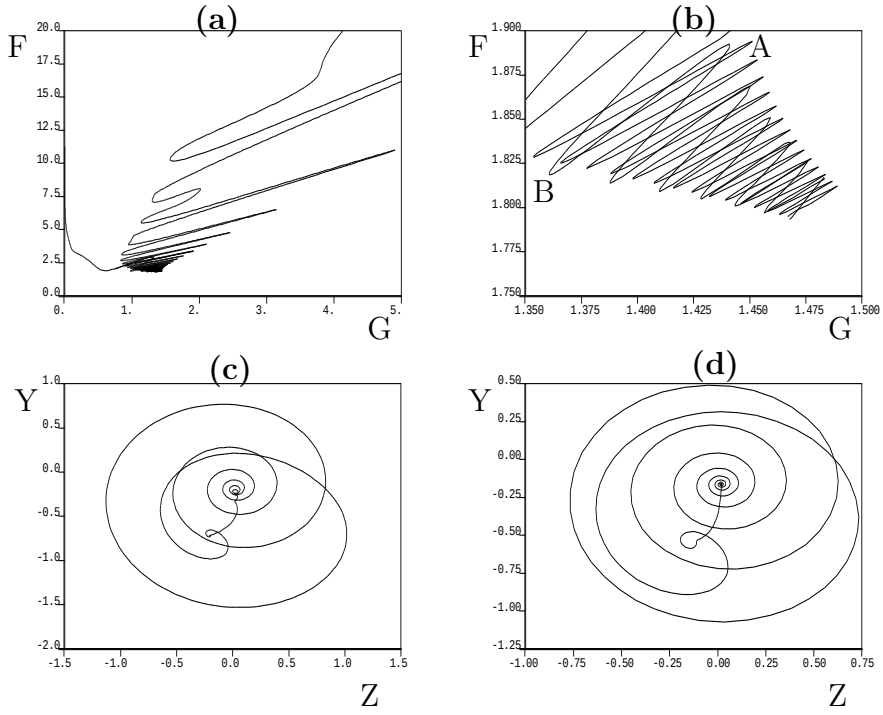


Fig. 10. (a) Homoclinic curves in the Lorenz model (4.11)-(4.13). (b) A zoom near the SNH point. (c) An orbit on branch A, which is homoclinic to the lower equilibrium. (d) An orbit on branch B, which is homoclinic to the upper equilibrium.

$F \to F_0$, $G \to G_0$, scale as

$$\mu_{n+1} - \mu_n \sim \frac{4\alpha}{\omega^2}(0.3075)\mu_n^2 = 0.244\mu_n^2.$$

This equation was used in drawing the curve showing the theoretical prediction in Fig. 11.

## 5 Conclusion

In this paper, we have extended the perturbation analysis of Gaspard [7] to get the precise asymptotics of the wiggly curves of primary homoclinic bifurcations emerging from a saddle-node/Hopf instability of type $s = -1$, $\alpha > 0$ (see equations (2.1), (2.2)). Our main result is the expressions we obtain for the amplitude of the oscillations in the homoclinic bifurcation curves (3.34) (with or without the superscript (3)) and for the frequency of oscillation (3.36) in the limit $\mu \to 0$, where $\mu$ is one of the parameters used to unfold the normal form for the instability. Gaspard found an expression for the homoclinic axis, i.e., a linear approximation to the homoclinic bifurcation curves arising from the SNH point, in the case of cubic perturbations to the normal form. We have been able to extend his results to the case of arbitrary analytic perturbations

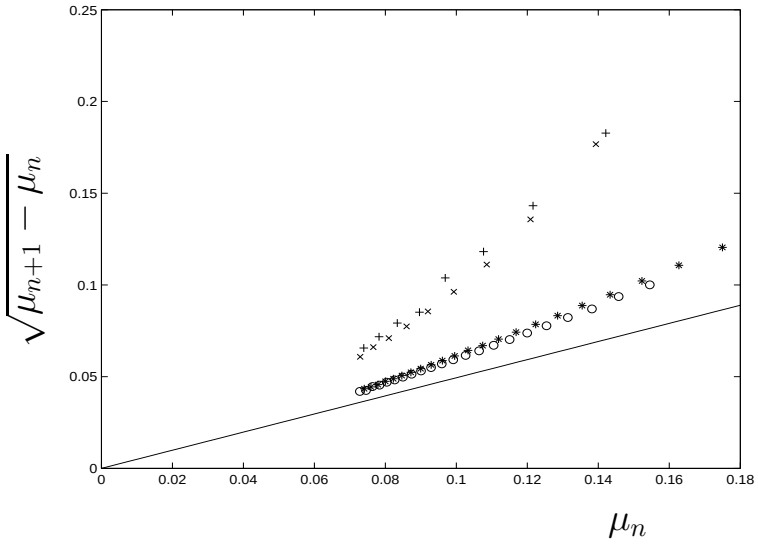


Fig. 11. Comparison of theory and numerics for the frequency of oscillation of the homoclinic bifurcations curves associated with the SNH point of the Lorenz model. The figure is drawn similarly to Fig. 7(a).

of the normal form, and to find the amplitude and frequency of the oscillations of the homoclinic bifurcation curves around the homoclinic axis.

The mechanism underlying the formation of wiggles in the homoclinic bifurcation curves has a simple geometric explanation. Specifically, consider the intersections of the stable and unstable manifolds of $P_+$ with the cylindrical surface $\Sigma^-$ (defined in section 3.3). $W^u(P_+) \cap \Sigma^-$ is a one-dimensional curve having one maximum and one minimum value of $z$ as $\Sigma^-$ is traversed, while $W^s(P_+) \cap \Sigma^-$ is a point (see Figure 4). As $\mu$ decreases the relative positions of $W^u(P_+) \cap \Sigma^-$ and $W^s(P_+) \cap \Sigma^-$ change. We defined a coordinate system in which $W^u(P_+) \cap \Sigma^-$ is stationary as $\mu$ varies and $W^s(P_+) \cap \Sigma^-$ sweeps out a curve on $\Sigma^-$. In this coordinate system, it is easily seen that if an intersection between $W^u(P_+) \cap \Sigma^-$ and $W^s(P_+) \cap \Sigma^-$ is to be maintained as $\mu$ is decreased (i.e., if we follow the homoclinic bifurcation curve toward the SNH instability) then we must alternately increase and decrease the other unfolding parameter, $\lambda$. This gives us the characteristic wiggly homoclinic bifurcation curves seen in two-parameter unfoldings of this instability.

We have compared our results with numerical studies of three systems with SNH instabilities, i.e., cubically perturbed normal form equations, a model for calcium wave propagation, and a low-order model for atmospheric circulation. We find qualitative and quantitative agreement between our theoretical predictions and the numerical results. Our analysis predicts that the two primary homoclinic bifurcation curves emerging from the SNH points will have the same frequency of oscillation in the limit of approach to the instability. Our numerical results are consistent with this prediction. However, we emphasise that our result is an asymptotic one, and that the two frequencies of oscillation

can be quite different away from the instability. This was particularly noticeable for the example in Sec. 4.3, where the data suggests the frequencies of oscillation do indeed converge to the theoretical limit, but that the quadratic correction is still large for $\mu = 0.1$. This of course serves to illustrate that in order to observe the true asymptotic scalings it is often hard to say a priori how small the unfolding parameter needs to be. Nevertheless, even for this example, the broad qualitative features predicted by the analysis – that there are two entwined wiggly curves – remains true in an $O(1)$ region of parameter space.

Our analysis also gives the leading-order exponential scaling of the envelope of the homoclinic bifurcation curves. In the case of cubically perturbed normal form equations, we were able to compare our prediction with numerical results and found good agreement as the SNH point was approached.

A further prediction of our analysis is that the difference in phase of the oscillations of the two homoclinic bifurcation curves can take any value. This prediction is consistent with the numerical examples in section 4. We have shown that the observation in [12] that the loci of homoclinic orbits to the two saddle-foci are precisely out of phase with each other is a property of the fact that only cubic perturbations to the normal form were considered in that paper.

Homoclinic bifurcations are of course just a part of the dynamics occurring near a SNH bifurcation, and are confined to an asymptotically thin wedge of the parameter space near the instability. Other studies have looked at other features of the dynamics, including the appearance of heteroclinic tangencies, quasi-periodic solutions and mode-locking when the normal form symmetry is broken (see, for instance, [7,12] and references therein). However, the appearance of homoclinic bifurcations through a SNH instability sometimes has major implications for the dynamics at parameter values far from the instability. For instance, in the example arising from calcium wave propagation discussed in section 4, homoclinic orbits in the system correspond to travelling pulses in an underlying partial differential equation model, and one of the SNH bifurcations in the example has a major role as an organising centre for the various curves of homoclinic orbits in the system [19,20].

One possible application of our work arises within the framework of numerical bifurcation analysis. It may be possible to numerically exploit the asymptotics we have developed for how the Shil'nikov homoclinic bifurcations emerge from the SNH point. This could lead to algorithms for starting homoclinic orbit continuation from an equilibrium point that undergoes a SNH codimension-two bifurcation. Such a philosophy was developed by Beyn [2] for starting homoclinic curves in the simpler case of a Takens–Bogdanov bifurcation (see also [3]).

Finally, note that we have focussed only on the location of homoclinic bifurcations near a SNH bifurcation, not on the dynamics associated with these homoclinic bifurcations. In fact, as others have shown, all the complicated dynamics normally associated with homoclinic bifurcations of saddle-foci can be found near SNH instabilities of this type. Specifically, in the case $0 < \alpha < 2$ in the normal form equations (2.1), (2.2), $P_+$ and $P_-$ are saddle-foci of Shil'nikov type, with associated horseshoe dynamics. Thus, we find a wedge of homoclinic chaos emerging (in parameter space) from the instability. Furthermore the homoclinic bifurcation to $P_+$ can occur within a trapping region in the phase space; there is an attractor in the region and it may be chaotic. We refer interested readers to Gaspard [7] for more details.

## Acknowledgements

ARC is indebted to the UK EPSRC for financial support to visit New Zealand under the terms of an Advanced Research Fellowship. We thank Yuri Kuznetsov for helpful comments and for showing us how to set $\beta = 0$ without loss of generality. We should also like to thank Nick Dudley-Ward for helping us through the fog of integral asymptotics, before we discovered the appropriate page of Gaspard's thesis.

## References

[1] N.J. Balmforth, G.R. Ierley, and E.A Spiegel. Chaotic pulse trains. *SIAM J. Appl. Math*, 54:1291–1334, 1994.

[2] W.-J. Beyn. Numerical analysis of homoclinic orbits emanating from a Takens–Bogdanov point. *IMA J. Numer. Anal.* 14:381–410, 1994.

[3] W.J. Beyn, A.R. Champneys, E.J. Doedel, W. Goverts, Yu.A. Kuznetsov, and B. Sandstede. Numerical continuation and computation of normal forms. In *Handbook of Dynamical Systems III: towards applications*, B. Fiedler (ed.), 149–220, Elsevier 1992.

[4] H.W. Broer and G. Vegter. Subordinate Shil'nikov bifurcations near some singularities of vector fields having low codimension. *Ergod. Theory Dynam. Sys.*, 4:509–525, 1984.

[5] E. Doedel, A. Champneys, T. Fairgrieve, Yu. Kuznetsov, B. Sandstede, and X. Wang. AUTO 97: Continuation and bifurcation software for ordinary differential equations. *http://indy.cs.concordia.ca/auto/main.html*

[6] P. Gaspard. *Tangences homoclines dans les systèmes dynamiques dissipatifs.* PhD thesis, Université Libre de Bruxelles, 1987.

[7] P. Gaspard. Local birth of homoclinic chaos. *Physica D*, 62:94–122, 1993.

[8] I.S. Gradshteyn and I.M. Ryzhik. *Tables of integrals, series and products.* Academic Press, New York, 1980.

[9] J. Guckenheimer. On a codimension two bifurcation. *Lecture Notes in Mathematics*, 898:99-142, D. Rand and L.-S. Young (eds). Springer Verlag, New York, 1981.

[10] J. Guckenheimer and P. Holmes. *Nonlinear Oscillations, Dynamical Systems and Bifurcations of Vector Fields.* Springer-Verlag, New York, U.S.A., second edition, 1986.

[11] V. Kirk. Breaking of symmetry in the saddle-node Hopf bifurcation. *Physics Letters A*, 154:243–248, 1991.

[12] V. Kirk. Merging of resonance tongues. *Physica D*, 66:267–281, 1993.

[13] Yu. A. Kuznetsov. *Elements of Applied Bifurcation Theory.* Springer-Verlag, New York, U.S.A., second edition, 1998.

[14] E.N. Lorenz. Irregularity - a fundamental property of the atmosphere. *Tellus A*, 36:98-110, 1984.

[15] M.M. Romeo and C.K.R.T. Jones. The stability of traveling calcium pulses in a pancreatic acinar cell. *Physica D*, 177:242–258, 2003.

[16] A. Shil'nikov, G. Nicolis, and C. Nicolis. Bifurcation and predictability analysis of low-order atmospheric circulation model. *International Journal of Bifurcation and Chaos*, 5:1701–1711, 1995.

[17] L.P. Shilnikov, A.L. Shilnikov, D.V. Turaev, and L.O. Chua. *Methods of Qualitative Theory in Nonlinear Dynamics, Part II* World Scientific, Singapore, 2001.

[18] J. Sieber. Numerical bifurcation analysis for multi-section semiconductor lasers. *SIAM J. Appl. Dyn. Sys.*, 1:248-270, 2002.

[19] J. Sim. Saddle-node/Hopf bifurcations in a physiological model. MSc thesis, University of Auckland, 2002.

[20] J. Sneyd, A. LeBeau, and D. Yule. Travelling waves of calcium in pancreatic acinar cells: model construction and bifurcation analysis. *Physica D*, 145:158–179, 2000.

[21] L. Van Veen, T. Opsteegh and F. Verhulst. Active and passive ocean regimes in a low-order climate model. *Tellus Series A – Dynamic Meteorology and Oceanography* 53:616–628, 2001

## A Evaluation of integrals

Here we derive the asymptotic estimate (3.10) for integrals of the form

$$\int_{-\infty}^{\infty} d\tau \frac{[\sinh(\tau)]^p}{[\cosh(\tau)]^\Lambda} e^{iK\tau/\sqrt{\mu}}, \tag{A.1}$$

where $\Lambda > p$ but is in general non-integer, $p$ is a non-negative integer, and $K \neq 0$ is a real constant that is independent of $\mu$.

Suppose to begin with that $K > 0$. Because even powers of $\sinh(\tau)$ can be written as polynomials in $\cosh\tau$, all cases can be reduced to one of the cases $p = 1$ and $p = 0$, with a change in $\Lambda$ if necessary. Further, the case $p = 1$ can be reduced to the case $p = 0$ as integration by parts yields

$$\int_{-\infty}^{\infty} d\tau \frac{\sinh(\tau)}{[\cosh(\tau)]^\Lambda} e^{iK\tau/\sqrt{\mu}} = \frac{iK}{(\Lambda-1)\sqrt{\mu}} \int_{-\infty}^{\infty} d\tau \frac{e^{iK\tau/\sqrt{\mu}}}{[\cosh(\tau)]^{\Lambda-1}}\,. \tag{A.2}$$

since $\Lambda \neq 1$.

The integral with $p = 0$ can be shown to have leading-order asymptotics

$$\int_{-\infty}^{\infty} \frac{e^{iK\tau/\sqrt{\mu}}}{[\cosh(\tau)]^\Lambda} d\tau \sim \frac{2\pi}{\Gamma(\Lambda)} \left(\frac{K}{\sqrt{\mu}}\right)^{\Lambda-1} e^{-\frac{K\pi}{2\sqrt{\mu}}} + o\left(\sqrt{\mu}^{1-\Lambda} e^{-\frac{K\pi}{2\sqrt{\mu}}}\right). \tag{A.3}$$

This estimate may be obtained by using the the known exact formula for the integral [8, 3.985.1]

$$\int_{-\infty}^{\infty} d\tau \frac{e^{iK\tau/\sqrt{\mu}}}{[\cosh(\tau)]^\Lambda} = 2^{\Lambda-1} \frac{\Gamma\left(\frac{\Lambda}{2} + i\frac{K}{2\sqrt{\mu}}\right)\Gamma\left(\frac{\Lambda}{2} - i\frac{K}{2\sqrt{\mu}}\right)}{\Gamma(\Lambda)}$$

and then approximating each of the Gamma functions using Stirling's formula (see [6, p.76]).

Combining (A.3) and (A.2), using properties of the Gamma function we find that the asymptotic expression for the integral (A.1) with $p = 1$ is just $i$ times that with $p = 0$

$$\int_{-\infty}^{\infty} d\tau \frac{\sinh(\tau)}{[\cosh(\tau)]^\Lambda} e^{iK\tau/\sqrt{\mu}} \sim \frac{2\pi i}{\Gamma(\Lambda)} \left(\frac{K}{\sqrt{\mu}}\right)^{\Lambda-1} e^{-\frac{K\pi}{2\sqrt{\mu}}} + o\left(\sqrt{\mu}^{1-\Lambda} e^{-\frac{K\pi}{2\sqrt{\mu}}}\right). \tag{A.4}$$

More generally, for $p > 1$, we can reduce to the case $p = 1$ or $p = 0$ by replacing even powers of $\sinh(\tau)$ in the integrand by the sum of even powers of $\cosh(\tau)$ plus a constant term. This constant term is $i^p$ and it provides the leading-order contribution to the integral. Hence we get the relation (3.10).

The case with $K < 0$ may be obtained from the case $K > 0$ by applying the transformation $\tau \mapsto -\tau$.

## B Analyticity of the homoclinic axis

Consider the expression for the homoclinic axis (3.41)

$$\lambda = h(\mu) = \sum_{m=1}^{\infty} h^{(2m+1)}(\mu) = -\frac{1}{2} \sum_{m=1}^{\infty} \mu^m K_0^{(2m+1)} \tag{B.1}$$

where the coefficients $K_0^{(2m+1)}$ come from the evaluation (3.39) of $I_{u0}^{(n)}$. The contribution to $K_0^{(2m+1)}$ from the term in $F$ with coefficient $c_{jkl}$ (for the case $j = k + 1, j + k + l = n = 2m + 1$) can be calculated using the formula (3.9) for $I_{u0}$, making use of (3.11) noting that $l$ is necessarily even. In particular, we find that the contribution from $c_{ijk}$ to

$$\sqrt{\pi} K_0^{(2m+1)} \frac{\Gamma(2 + 1/\alpha)}{\Gamma(3/2 + 1/\alpha)}$$

is

$$\begin{aligned} k_{ijk} &:= \frac{2}{\alpha} \mathrm{Re}(c_{jkl})(\alpha + 1)^j \int_{-\infty}^{\infty} \frac{[\sinh(\tau)]^l}{[\cosh(\tau)]^{n+1+2/\alpha}} d\tau \\ &= \frac{2\sqrt{\pi}}{\alpha} \mathrm{Re}(c_{jkl})(\alpha + 1)^j \sum_{s=0}^{l/2} \begin{pmatrix} l/2 \\ s \end{pmatrix} (-1)^s \frac{\Gamma\left(\frac{n+1-l+2s}{2} + \frac{1}{\alpha}\right)}{\Gamma\left(\frac{n+2-l+2s}{2} + \frac{1}{\alpha}\right)}. \end{aligned}$$

where $\begin{pmatrix} l/2 \\ s \end{pmatrix}$ is the binomial coefficient. The ratio of the $\Gamma$ functions in each term in the sum is strictly less than 1. Therefore, after summing the binomial coefficients we have that

$$|k_{ijk}| < \frac{2\sqrt{\pi}}{\alpha} |\mathrm{Re}(c_{jkl})| (\alpha + 1)^j 2^{l/2} \leq [2(1 + \alpha)]^m \tilde{c}_m \tilde{M}(\alpha)$$

where $\tilde{c}_m$ is the maximum modulus of all the $c_{ijk}$ being considered and $\tilde{M}(\alpha)$ is an $m$-independent constant. There are $m + 1$ such terms contributing to

$K_0^{(2m+1)}$. Similar calculations show that the term proportional to $d_{jkl}$ ($j = k, j+k+l = n = 2m+1$) has a similar bound, and there are $m+1$ such terms. Hence

$$|K_0^{(2m+1)}| \leq (2m+2)c_m[2(1+\alpha)]^m M(\alpha)$$

where $c_m$ is the maximum modulus of all the coefficients $c_{ijk}$ and $d_{ijk}$ contributing to the term $K_0^{(2m+1)}$ and $M(\alpha)$ is some $m$-independent constant.

Now, since the Taylor series for $F$ and $G$ converge with a finite radius of convergence, $R$ say, we have $c_m \leq KR^{-2m}$ for some bounded positive constant $K$. Hence, for $m$ sufficiently large we have

$$\left|K_0^{(2m+1)}\right| \leq KM(\alpha)\left(\frac{4(1+\alpha)}{R^2}\right)^m.$$

Thus, the power series (B.1) represents a convergent Taylor series with radius of convergence $|\mu| \leq R^2/4(1+\alpha)$.